KONINKLIJK BELGISCH INSTITUUT VOOR NATUURWETENSCHAPPEN
OD NATUUR – BEHEERSEENHEID VAN HET MATEMATISCH MODEL

MOnitoring en MOdellering van het cohesieve sedimenttransport en evaluatie van de effecten op het mariene ecosysteem ten gevolge van bagger- en stortoperatie (MOMO)

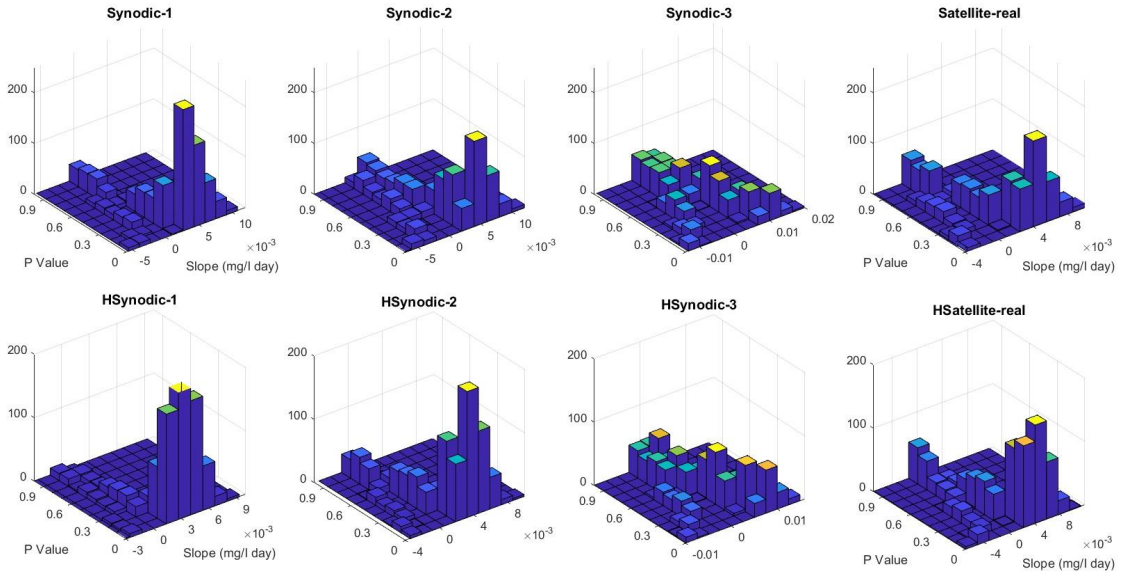

Activiteitsrapport (1 juli - 31 december 2022)

Michael Fettweis, Xavier Desmit

MOMO/10/MF/202303/NL/AR/2

museum
Operational Directorate Natural Environment
OD Nature I OD Natuur I DO Nature

KBIN-OD Natuur - BMM
Vautierstraat 29
B–1000 Brussel
België

Inhoudstafel

1. Inleiding

1.1. Voorwerp van deze opdracht

Het MOMO-project (monitoring en modellering van het cohesieve sedimenttransport en de evaluatie van de effecten op het mariene ecosysteem ten gevolge van bagger- en stortoperatie) maakt deel uit van de algemene en permanente verplichtingen van monitoring en evaluatie van de effecten van alle menselijke activiteiten op het mariene ecosysteem waaraan België gebonden is overeenkomstig het verdrag inzake de bescherming van het mariene milieu van de noordoostelijke Atlantische Oceaan (1992, OSPAR-Verdrag). De OSPAR Commissie heeft de objectieven van haar Joint Assessment and Monitoring Programme (JAMP) gedefinieerd tot 2021 met de publicatie van een holistisch "quality status report" van de Noordzee en waarvoor de federale overheid en de gewesten technische en wetenschappelijke bijdragen moeten afleveren ten laste van hun eigen middelen.

De menselijke activiteit die hier in het bijzonder wordt beoogd, is het storten in zee van baggerspecie waarvoor OSPAR een uitzondering heeft gemaakt op de algemene regel "alle stortingen in zee zijn verboden" (zie OSPAR-Verdrag, Bijlage II over de voorkoming en uitschakeling van verontreiniging door storting of verbranding). Het algemene doel van de opdracht is het bestuderen van de cohesieve sedimenten op het Belgisch Continentaal Plat (BCP) en dit met behulp van zowel numerieke modellen als het uitvoeren van metingen. De combinatie van monitoring en modellering zal gegevens kunnen aanleveren over de transportprocessen van deze fijne fractie en is daarom fundamenteel bij het beantwoorden van vragen over de samenstelling, de oorsprong en het verblijf ervan op het BCP, de veranderingen in de karakteristieken van dit sediment ten gevolge van de bagger- en stortoperaties, de effecten van de natuurlijke variabiliteit, de impact op het mariene ecosysteem in het bijzonder door de wijziging van habitats, de schatting van de netto input van gevaarlijke stoffen op het mariene milieu en de mogelijkheden om deze laatste twee te beperken.

Een samenvatting van de resultaten uit de vergunningsperioden 2017-2021 kan gevonden worden in het "Vooruitgangsrapport (juni 2019) over de effecten op het mariene milieu van baggerspeciestortingen" (Lauwaert et al. 2019) en het Syntheserapport over de effecten op het mariene milieu van baggerspeciestortingen" (Lauwaert et al., 2021) die gepubliceerd werden conform art. 10 van het K.B. van 12 maart 2000 ter definiëring van de procedure voor machtiging van het storten in de Noordzee van bepaalde stoffen en materialen.

1.2. Algemene doelstellingen

Het onderzoek uitgevoerd in het MOMO project kadert in de algemene doelstellingen om de baggerwerken op het BCP en in de kusthavens te verminderen, om de effecten van het storten van baggerspecie te kwantificeren en om een gedetailleerd inzicht te verwerven van de fysische processen die plaatsvinden in het mariene kader waarbinnen deze baggerwerken worden uitgevoerd. Dit impliceert enerzijds beleidsondersteunend onderzoek naar de vermindering van de sedimentatie op de baggerplaatsen en het evalueren van alternatieve stortmethoden. Anderzijds is vernieuwend onderzoek noodzakelijk om beter de effecten van het storten van baggerspecie in te schatten. Dit onderzoek is specifiek gericht op het dynamische gedrag van slib in de waterkolom en op de bodem en de interacties tussen fysische en biologische processen en zal uitgevoerd worden met behulp van modellen, in situ metingen en remote sensing data.

De specifieke acties die binnen dit onderzoek uitgevoerd worden om de algemene doelstellingen in te vullen zijn:

1. Streven naar een efficiënter stortbeleid door een optimalisatie van de stortlocaties.

2. Continue monitoring van het fysisch en biogeochemisch milieu waarbinnen de baggerwerken worden uitgevoerd (Taak 1) en aanpassing van de monitoring aan de nog op te stellen targets voor het bereiken van de goede milieutoestand (GES), zoals gedefinieerd zal worden binnen MSFD;

3. Uitbouw en optimalisatie van het numerieke modelinstrumentarium, ter ondersteuning van het onderzoek (Taak 2.1).

1.3. Algemeen Onderzoek 2012-2026

Het onderzoek heeft als doel om de effecten van baggerspeciestortingen op het mariene ecosysteem (fysische en biogeochemische aspecten) te onderzoeken. Hiervoor worden in situ metingen verzameld, gebruik gemaakt van remote sensing data en worden numerieke modellen ingezet. Voor de vergunningsperiode 2022-2026 worden volgende taken voorzien:

1) In situ en remote sensing metingen en data-analyse

De monitoring van effecten van baggerspeciestortingen gebeurd met behulp van een vast meetstation in de nabijheid van MOW1, en met meetcampagnes met de RV Belgica (een 10-tal meetcampagnes voor het verzamelen van traject informatie, profielen en de calibratie van sensoren; en een 10-tal campagnes voor het onderhoud van het meetstation te MOW1). De geplande monitoring is gericht op het begrijpen van processen, zodoende dat de waargenomen variabiliteit en de effecten van baggerspeciestortingen in een correct kader geplaatst kunnen worden. Een belangrijk deel is daarom gericht op zowel het uitvoeren van de in situ metingen, het garanderen van kwalitatief hoogwaardige data en het archiveren, rapporteren en interpreteren ervan. Remote sensing data afkomstig van onder andere satellieten worden gebruikt om een ruimtelijk beeld te bekomen.

2) Uitbouw en optimalisatie van het modelinstrumentarium

Het tijdens de voorbije jaren verbeterde en aangepaste slibtransportmodel zal verder worden ontwikkeld. Dit zal parallel gebeuren met de nieuwe inzichten die voorvloeien uit de metingen en de procesgerichte interpretatie van de metingen.

3) Ondersteunend wetenschappelijke onderzoek

Monitoring gebaseerd op wetenschappelijke kennis is essentieel om de effecten van menselijke activiteiten (hier het storten van baggerspecie) te kunnen inschatten en beheren. Om te kunnen voldoen aan de door OSPAR opgelegde verplichtingen van monitoring en evaluatie van de effecten van menselijke activiteiten is het ontwikkelen van nieuwe monitorings- en modelleractiviteiten nodig. Dit houdt in dat onderzoek dat de actuele stand van de wetenschappelijke kennis weerspiegelt wordt uitgevoerd en dat de hieruit voortvloeiende nieuwe ontwikkelingen geïntegreerd zullen worden in zowel de verbetering van het modelinstrumentarium als voor het beter begrijpen van het kustnabije ecosysteem.

1.4. Onderzoek Januari 2022 – December 2024

Voor de periode 2019-2021 werd rekening gehouden werd met de aanbevelingen voor de minister ter ondersteuning van de ontwikkeling van een versterkt milieubeleid zoals geformuleerd in het “Syntheserapport over de effecten op het mariene milieu van baggerspeciestortingen (2021)” dat uitgevoerd werd conform art. 10 van het K.B. van 12 maart 2000 ter definiëring van de procedure voor machtiging van het storten in de Noordzee van bepaalde stoffen en materialen.

Taak 1: In situ en remote sensing metingen en data-analyse

Taak 1.1 Langdurige metingen te MOW1 en W05

Sinds eind 2009 worden er continue metingen uitgevoerd te MOW1 met behulp van een meetframe (tripode). Met dit frame worden stromingen, slibconcentratie, korrelgrootte-verdeling van het suspensiemateriaal, saliniteit, temperatuur, waterdiepte en zeebodem altimetrie gemeten. Om een continue tijdreeks te hebben, wordt gebruik gemaakt van 2 tripodes. Na ongeveer 1 maand wordt de verankerde tripode voor onderhoud aan wal gebracht en wordt de tweede op de meetlocatie verankerd. Op de meetdata wordt een kwaliteitsanalyse uitgevoerd, zodat de goede data onderscheiden kunnen worden van slechte of niet betrouwbare data.

Veranderingen in kustnabije ecosystemen zijn dikwijls gecorreleerd met veranderingen van de helderheid van het water of de concentratie aan particulair suspensiemateriaal (SPM) en dus ook met het gehalte aan particulair organisch materiaal. De zone waar de invloed van het minerale en kustnabij suspensiemateriaal overgaat in een zone met dominantie van organisch suspensiemateriaal van mariene origine is van bijzonder belang. De monitoring wordt uitgebreid met de verankering van een meetboei in locatie W05 (51°N 24.96', 2°E 48.7'). W05 is één van de drie monitoringspunten waar waterstalen en sensormetingen maandelijks worden uitgevoerd.

Taak 1.2 Calibratie van sensoren tijdens in situ metingen

Tijdens meetcampagnes met de R/V Belgica zullen een voldoende aantal 13-uursmetingen uitgevoerd worden met als hoofddoel het kalibreren van optische of akoestische sensoren en het verzamelen van verticale profielen. De metingen zullen plaatsvinden in het kustgebied van het BCP (MOW1, W05). De optische metingen (Optical Backscatter Sensor) zullen gekalibreerd worden met de opgemeten hoeveelheid materie in suspensie (gravimetrische bepalingen na filtratie) om te komen tot massa concentraties

Taak 1.2 Bio-geo-chemische monitoring van het SPM (BGCMonit)

SPM bestaat uit minerale deeltjes van fysicochemische (b.v. kleimineralen, kwarts, veldspaat) en biogene oorsprong (b.v. calciet, aragoniet, opaal), levend (bacteriën, fyto- en zoöplankton) en niet-levend organisch materiaal (b.v. fecale pellets, detritus, exopolymeren), en partikels van menselijke oorsprong (microplastiek). Het SPM kan door hydrofobe organische polluenten of metalen gecontamineerd zijn. De samenstelling en concentratie van het SPM inclusief de hydrofobe polluenten verandert in functie van de tijd en de locatie. Deze variaties worden beïnvloed door de interacties tussen de fysische processen (getij, meteo, klimaat), biologische cycli (algenbloei), chemische processen (koolstofcyclus) en menselijke activiteiten (aanvoer van nutriënten, bagger- en stortactiviteiten, offshore constructies). De samenstelling van het particulair en opgelost suspensiemateriaal zal bepaald worden tijdens meetcampagnes met de RV Belgica tijdens een 10-tal campagnes per jaar. Naast de totale hoeveelheid aan SPM worden ook de concentraties aan verschillende organische bestanddelen (POC, PON, TEP, chlorofyl en phaeofytine) bepaald. De opgeloste stoffen zijn inorganische nutriënten, DOC, DIC en alkaliniteit. Stalen van suspensiemateriaal zullen genomen worden met de centrifuge om de samenstelling ervan te bepalen.

Taak 1.4: Archivering en verwerking van de data

De meetdata worden gearchiveerd en er wordt een kwaliteitsanalyse uitgevoerd, zodat de goede data onderscheiden kunnen worden van slechte of niet betrouwbare data. Slechte data kunnen bv optreden doordat het instrument slecht heeft gewerkt en verkeerd werd ingesteld. Niet betrouwbare data zijn typisch geassicieerd met bv biofouling. De data en metadata worden gearchiveerd. De metingen worden verwerkt en geïnterpreteerd. En

zullen dienen als basis voor het verder gebruik bij wetenschappelijke vraagstellingen.

Taak 2: Uitbouw en optimalisatie van het modelinstrumentarium

Taak 2.1: Opstellen van een slibtransportmodel voor het BCP met Coherens V2

Een slibtransportmodel zal worden geïmplementeerd met de software Coherens V2. De software laat toe om rekening te houden met gemengde sedimenten en dus met de interactie tussen zand en slib en laat morfologische berekeningen toe door een verbeterde implementatie van het schema voor het massabehoud en gebruik van lagen met gemengde sedimenten. Verdere aanpassingen en verbeteringen aan het model zullen worden uitgevoerd, meer bepaald:

- Kritische bodemschuifspanning voor erosie van gemengde sedimenten,
- Formulering voor de bodemschuifspanning,
- Koppeling van het model met het TILES voxel model voor een betere voorstelling van de bodemkarakteristieken.

Taak 2.2: Validatie van het slibtransportmodel voor het jaar 2013 (stortproef)

Een eerste toepassing van het model kan het jaar 2013 zijn, waarin de terreinproef voor alternatieve stortplaats alsook een intensieve monitoring plaatsvond. Deze laatste zal gebruikt worden voor de validatie van het model. Verder zal het model vergeleken worden met andere modellen van het BCP.

Taak 2.3: Optimalisatie baggerwerken

Een operationeel stortmodel zal worden opgezet in overleg met aMT. Dit model zal geïntegreerd worden in de binnen BMM-OD Natuur beschikbare operationele modellen. Het model zal gebruikt worden om in functie van de voorspelde fysische (wind, stroming, golven, sedimenttransport, recirculatie), economische (afstand, grootte baggerschip) en ecologische aspecten op korte termijn een keuze te kunnen maken tussen de beschikbare stortlocaties. Een eerste test hiervoor werd uitgevoerd in Van den Eynde en Fettweis (2011) waarin werd aangetoond dat door een optimale positie te kiezen voor het storten van baggerspecie in functie van de meteorologische omstandigheden, een vermindering van de aanslibbing van de vaargeulen en haven van Zeebrugge kan worden verwacht.

Het model zal worden gebruikt voor de optimalisatie van de baggerwerken. Verschillende simulaties kunnen worden uitgeoefend waarbij de invloed van de verschillende mogelijke stortplaatsen kunnen worden geëvalueerd.

Taak 2.4: Flocculatiemodel

De inzichten die voortvloeien uit de in situ data (Taken 1.4, 3.1 en 3.2) zullen worden geïntegreerd in een numeriek model dat het verband tussen SPM, TEP en flocculatie langsheen temporele (getij, seizoenen) en geografische (waterkolom, onshore-offshore) schalen combineert. Het model zal worden opgezet als 1D verticaal en zal gekoppeld worden met het 2 klassen populatie model van Lee et al. (2011). Hierdoor zal de verticale verdeling van de minerale en de organische fractie van het SPM en hun interactie kunnen worden voorspeld.

Taak 3: Ondersteunend wetenschappelijk onderzoek

Monitoring gebaseerd op wetenschappelijke kennis is essentieel om de effecten van menselijke activiteiten (hier het storten van baggerspecie) te kunnen inschatten en beheren. Om te kunnen voldoen aan de door OSPAR opgelegde verplichtingen van monitoring en evaluatie van de effecten van menselijke activiteiten is een verdere implementatie van huidige en het ontwikkelen van nieuwe monitoringsactiviteiten nodig. Meer specifiek gericht op de activiteit ‘storten van baggerspecie’ worden hier – wat het fysische milieu betreft - turbiditeit, samenstelling van de zeebodem, bathymetrie en

hydrografische condities beoogt. Deze taak speelt hierop in door de ontwikkeling en de implementatie van nieuwe tools die de actuele stand van de wetenschappelijke kennis weerspiegelen teneinde de mathematische modellen te optimaliseren en verfijnen.

Taak 3.1: SPM samenstelling - minerale fractie

Door de aanwezigheid van gemengde sedimenten in de zeebodem (zand en slib) zal tijdens sterke stroming en of hoge golven ook een gemengde minerale fractie in suspensie komen. Dit heeft twee consequenties voor monitoring. Ten eerste reageren akoestische en optische sensoren verschillend op zand en slib, zodat de verzamelde tijdreeksen een grotere onnauwkeurigheid hebben tijdens zo'n momenten (Fugate & Friedrichs, 2002; Baschek et al., 2017; Schwarz et al, 2017; Fettweis et al., 2019). Ten tweede bevatten zandkorrels geen mineraal-gebonden organisch materiaal en stalen genomen tijdens dit soort momenten kunnen dus de onzekerheid van het SPM-POM model vergroten. Indien er geen rekening gehouden wordt hiermee zal de SPM concentratie onder- of overschat worden alsook de afgeleid organische fracties. Doel is om de zand en slibfractie te identificeren door gebruik te maken van innovatieve meettechnieken (Pearsons et al., 2021) die optische en akoestische sensoren combineren. Het ultieme doel is om te komen tot tijdreeksen van zand- en slibconcentratie te MOW1.

Uit visuele inspecties van de bodemsamenstelling te MOW1 tijdens de laatste jaren blijkt dat het sediment zandiger is geworden. De hypothese is, dat dit verband houdt met erosie van de vooroever na de strandopspuitingen die de voorbije jaren werden uitgevoerd. Aan de hand van de boven aangehaalde methode zal nagegaan worden of er een trend naar zandaanrijking kan vastgesteld worden in de omgeving van MOW1.

Taak 3.2: SPM samenstelling - organische fractie

Het semi-empirisch POM-SPM model (Fettweis et al., 2022) zal verfijnd worden met de nieuwe data verzameld in taak 1.3. Hierdoor zal de inschatting van de minerale en de vers en mineraal-gebonden organische fractie nauwkeuriger kunnen worden gedaan.

Op basis van dit POM-SPM model kan de samenstelling van het suspensiemateriaal (minerale fractie, vers en mineraal gebonden POC, PON en TEP) worden berekend voor de tijdreeksen te MOW (vanaf 2005) en voor de satellietdata (vanaf 1997). Dit zal toelaten om de geografische en temporele variabiliteit van de transitiezone tussen het kustgebonden turbiditeitsmaximum en de offshore wateren te kwantificeren. De dynamica van het suspensiemateriaal in beide gebieden is verschillend, wat consequenties heeft naar de modellering ervan. Verder kan uit de lange tijdsreeksen gekeken worden of het gebruik van de stortplaatsen, meer bepaald S1, geleid heeft tot een zeewaartse uitbreiding van het turbiditeitsmaximum.

Taak 3.3: Trends in SPM concentratie

Om significante statistische trends te kunnen documenteren in SPM concentratie over de laatste decades, zijn metingen nodig die een lange tijdspanne omvatten en een groot gebied omvatten. Deze data zijn helaas niet beschikbaar. Wat er wel beschikbaar is zijn de tripode metingen te MOW1 (vanaf 2005) en op andere locaties, de puntmetingen verzameld met onderzoeksschepen in het Belgisch Deel van de Noordzee sinds ongeveer 1970 (cf. Belspo 4DEMON project) en satellietbeelden (vanaf 1997). De tripode data geven de temporele variabiliteit weer, maar zijn heel beperkt wat ruimtelijke spreiding betreft. De 4DEMON en satellietbeelden zijn beschikbaar over een lange periode en over een groot gebied, maar kunnen de temporele schaal niet oplossen. Om deze heterogene datasets samen te kunnen gebruiken, zal gekeken worden naar de statistische verschillen tussen de datasets en naar een manier om deze te combineren. Doel is om mogelijke trends in de SPM concentratie te identificeren en deze te linken aan natuurlijke veranderingen of aan menselijke activiteiten.

De trendanalyse van de historische data zal de basis vormen om de verandering van de SPM concentratie in de nabijheid van de nieuwe stortplaats ZBW te kwantificeren.

Taak 4: Rapportage en outreach

Om de zes maanden zal er een activiteitenrapport worden opgesteld dat de onderzoeksresultaten beschrijft. Jaarlijks wordt er een 'factual data' rapport opgesteld van de verzamelde meetgegevens. De resultaten uit het onderzoek zullen tevens worden voorgesteld op workshops, conferenties en in de wetenschappelijke literatuur.

1.5. Gerapporteerde en uitgevoerde taken

Periode Januari 2022– Juni 2022

Taak 1.1: De meetreeks te MOW1 werd verdergezet.

Taak 1.2: Calibratie van OBS sensoren werd uitgevoerd tijdens RV Begica campagnes 2022/01, 2022/03, 2022/06, 2022/09 en 2022/14.

Taak 3.1: De akoestische en optische sensoren werden gebruikt om veranderingen in sedimentsamenstelling te zien te MOW1. Eerste resultaten worden getoond in hoofdstuk 2.

Taak 3.2: Intensieve bio-geochemische monitoring werd uitgevoerd te MOW1, W05 en W08 tijdens RV Belgica campagnes 2022/01, 2022/03, 2022/07, 2022/11, 2022/14). Eerste resultaten worden besproken in hoofdstuk 3.

Periode Juli 2022– December 2022

Taak 1.1: De meetreeks te MOW1 werd verdergezet.

Taak 1.2: Calibratie van OBS sensoren werd uitgevoerd tijdens RV Begica campagnes 2022/17, 2022/19, 2022/21, 2022/24, 2022/28 en 2022/32.

Taak 2.4: De interactie van phytoplankton en SPM resulteert in de vorming van grotere vlokken met hogerer valsnelheden. In een labo experiment werd de flocculatie bestudeerd tussen klei en phytoplankton deeltjes. Een twee-klassen flocculatiemodel werd opgesteld om de experimentele data kwantitatief te analyseren, zie paper in appendix 1.

Taak 3.2: Intensieve bio-geochemische monitoring werd uitgevoerd te MOW1, W05 en W08 tijdens RV Belgica campagnes 2022/17, 2022/19, 2022/21, 2022/24, 2022/28 en 2022/32). Eerste resultaten worden besproken in hoofdstuk 3.

Taak 3.3: De informatieverlies van niet continue tijdreeksen werd bepaald. Dit zal de basis vormen voor de trendanalyse in SPM concentratie over een langere periode, zie hoofdstuk 2.

1.6. Publicaties (Januari 2022 – December 2026)

Hieronder wordt een overzicht gegeven van publicaties met directe betrokkenheid van het KBIN waar resultaten en data uit het MOMO project in werden gebruikt.

Activiteits-, Meet- en Syntheserapporten

Fettweis M, Desmit X. 2023 MOMO activiteitsrapport (1 juli – 31 december 2022). BMM-rapport MOMO/10/MF/202303/NL/AR/2, 27pp + app.

Fettweis M, Baeye M, Desmit X. 2022 MOMO activiteitsrapport (1 januari – 30 juni 2022). BMM-rapport MOMO/10/MF/202210/NL/AR/1, 21pp + app.

Conferenties/Workshops

Baeye M, Delhaye L, Fettweis M. 2022. Acoustic and optical turbidity response to altering particle size distribution during extreme events. EuroSea/OceanPredict workshop, 29 June – 1 July, Exeter (UK).

Fettweis M, Desmit X, Terseleer N, Parmentier K, Van der Zande D, Schartau M, Lee BJ, Riethmüller R. 2022. The characteristics of the organic matter in biomineral flocs. Ocean Science Meeting, 24 February – 4 March, Honolulu (USA).

Peer reviewed artikels

Escobar S, Bi Q, **Fettweis M,** Monbaliu J, Wongsoredjo S, Toorman E. 2023. A 2DH flocculation model for coastal domains. Ocean Dynamics (in revision)

Fettweis M, Riethmüller R, Van der Zande D, Desmit X. Water quality monitoring in coastal seas: How significant is the information loss of patchy time series? Science of the Total Environment 873, 162273. doi:10.1016/j.scitotenv.2023.162273.

Fettweis M, Schartau M, Desmit X, Lee BJ, Terseleer N, Van der Zande D, Parmentier K, Riethmüller R. 2022. Organic matter composition of biomineral flocs and its influence on suspended particulate matter dynamics along a nearshore to offshore transect. Journal of Geophysical Research Biogeosciences, 126, e2021JG006332. doi:10.1029/2021JG006332

Ho NQ, Fettweis M, Hur J, Desmit X, Kim JI, Jung DW, Lee SD, Lee S, Choi YY, Lee BJ. 2022. Flocculation kinetics and mechanisms of microalgae- and clay-containing suspension in different microalgae growth phases. Water Research 226, 119300. doi:10.1016/j.watres.2022.119300

Ho QN, Fettweis M, Spencer KL, Lee BJ. 2022. Flocculation with heterogeneous composition in water environments: A review. Water Research. 118147. doi:10.1016/j.watres.2022.118147

2. Sample based water quality monitoring of coastal seas: How significant is the information loss in patchy time series compared to continuous ones?

The purpose of water quality monitoring in marine waters is multiple. From a policy perspective it may consist in identifying pollutant concentrations exceeding their threshold value, detecting harmful algae blooms, evaluating the ecological status of an area, or detecting trends. From a scientific perspective the data may be used to quantify the mean biogeochemical properties of a system, evaluating variations at different time scales, understanding the element cycles and their underlying processes and validating model predictions related to major trends such as global warming or the discharge of nutrients into the sea. These objectives require a long time series of water quality data that will also help policy to develop effective strategies for mitigation in case for example of eutrophication, effects of human activities at sea or accidental pollution (Lovett et al., 2007; Conley et al., 2009; Kirby and Law, 2010; Mack et al., 2020). Measurements from a monitoring program that rely on water sampling from a vessel or on remote sensing data are limited to moderate and in the latter case cloud free meteorological and oceanographic conditions. It is thus essential to assess the representativeness of such a subsample of the data population and to evaluate the information loss provided by patchy and discrete sampling (e.g., Erkkilä and Kalliola, 2007; Anttila et al. 2012; Lin et al., 2022).

In this study, three water quality parameters are considered: turbidity, which is controlled by the concentration, size, and composition of suspended particulate matter (SPM), the flux of SPM and chlorophyll a (Chl) concentration as a proxy for phytoplankton abundance. They are representative for key processes in the food web and element cycling on shelf seas on different time scales: a vertical resuspension-deposition pattern of SPM on the scale of tides and in many areas waves on the scale of low pressure passages, a directional pattern of horizontal SPM fluxes governed by variations in ebb-flood currents, and a seasonal pattern of Chl concentration that is controlled by primary production and grazing. Other particulate water quality parameters fit into these types of variability, such as particulate organic matter (POM) concentration, pollutants adsorbed to clay minerals and the transport of microplastics and pollutants. Turbidity is the oldest water quality parameter; the first standardized method used Secchi disks and dates back to the 19th century (Wernand, 2010). Today, water sampling, optical back- or side scatter sensors, acoustic backscatter sensors and satellites provide data on SPM concentration (e.g., Grabemann and Krause, 1989; Druine et al., 2018). Chl is correlated with the phytoplankton biomass and thus with the particulate organic matter (POM) pool; it can be obtained directly from water samples, indirectly by fluorometers (Roesler et al., 2017) and satellite observations (Harvey et al., 2015). The SPM concentration may further act as a proxy for the organic components, such as the content of POM in the SPM; and the concentration of particulate organic carbon (POC), particulate organic nitrogen (PON) and transparent exopolymer particles (TEP) (Keil et al., 1994; Ransom et al., 1998; Schartau et al., 2019; Fettweis et al., 2022), or for the occurrence of trace metals or organic pollutants adsorbed onto clay minerals (Kowalska et al., 1994; Gaulier et al., 2019).

The data from water samples or from satellites provide a distorted image of the continuous variability as they consist of time series at low-frequent discrete time intervals, which are in contrast with high-frequent time series from buoys or landers that incorporate all relevant amplitudes in the variations. The study focuses on coastal areas in the North Sea, where hydrodynamics are dominated by tides. The main frequencies of variability are quarter-diurnal (about 6.2 hours), semidiurnal (12.4 hours), half-synodic (14.7 days) and

synodic (29.5 days). Further the effect of biology is responsible for seasonal variations. Additional variations have lower (interannual variations) or higher frequencies (turbulence) or occur irregularly such as variations caused by extreme weather events or human activities. The three parameters vary along all these time scales due to their fast response to changes in physical forces, whether caused by astronomical (tides, seasons), climatological or human effects or nutrient and light availability. The objectives of the study are to understand the effect of a sampling scheme and thus the frequency of the sampling on the information that is collected. We have used high-frequency data as a sufficient approximation to a continuous time series of SPM, SPM flux and Chl concentration from a tidally dominated coastal area to answer the significance of information loss in relation to lower-sampling schemes, and the effect of this sampling on the detection of interannual trends.

2.1. Methods

2.1.1. Continuous time series

In order to evaluate the loss of information due to discrete sampling and the representativeness of a sampling scheme, we have used the 2013 high-frequency (Δt=15 minutes) time series of calibrated Optical Backscatter Sensor (OBS) derived SPM concentration and ADCP derived current velocity data from MOW1 station located in the southern Bight of the North Sea (Fettweis et al., 2016). SPM flux has been calculated as the product of the SPM concentration and the current velocities and is expressed as kg/m²s. The fluorescence data were recorded in spring 2016 and summer 2017 in the same station. Fluorescence was converted to Chl concentration (expressed in µg/l) using the factory specifications of the Eco-FL sensor (Sea-Bird Electronics, 2011). The data have been collected at the MOW1 coastal observatory located in the Belgian nearshore area (51°N 21.30', 3°E 07.85') at 2 m above the bed. The average water depth is about 12 m. Located some 5 km away from the shoreline it is situated within a coastal turbidity maximum area where SPM concentrations vary between 20 mg/l and more than 3000 mg/l at 2 m above the bed. The Belgian nearshore is characterized by semidiurnal tides with a mean tidal amplitude of 3.6 m. The tidal current ellipses are elongated and vary on average between 0.2 and 0.8 m/s during spring tide and 0.2 and 0.5 m/s during neap tide at 2 m above the bed. The strong tidal currents, the shallowness and the low freshwater discharges result in a well-mixed water column. The residual alongshore currents and the residual SPM fluxes at MOW1 are, respectively, in 53% and 80% of the time directed towards the NE, which occur during periods of prevailing SW winds.

Both the SPM concentration and flux time series from MOW1 consists of 27849 data distributed over the four seasons, while the Chl concentration time series counts 12574 data distributed over spring and summer. Although the Chl time series covers only 35% of the year, it incorporates critical periods, that is, spring and summer but does not include other periods, such as the start of the bloom in February and the late summer/early autumn bloom. Therefore, a true annual mean cannot be derived from it. Figure 2.1 shows the time series of SPM and Chl concentrations, and of SPM flux at MOW1 together with the tidal amplitude. Additionally, the mean over a certain period (can be synodic or half-synodic) is shown in the figure and is considered as the true mean.

Additionally, the 2010 time series (Δt=120 minutes, 3906 data) of turbidity (algae and non-algae) from the West Gabbard smart buoy (51°N 58.82'; 2°E4.97') was used as an example of a location with lower turbidity. The turbidity is about ten times lower than at MOW1 and the time series was used in this study only for trend detection. West Gabbard is located in well-mixed conditions in about 30 m water depth at 36 km offshore.

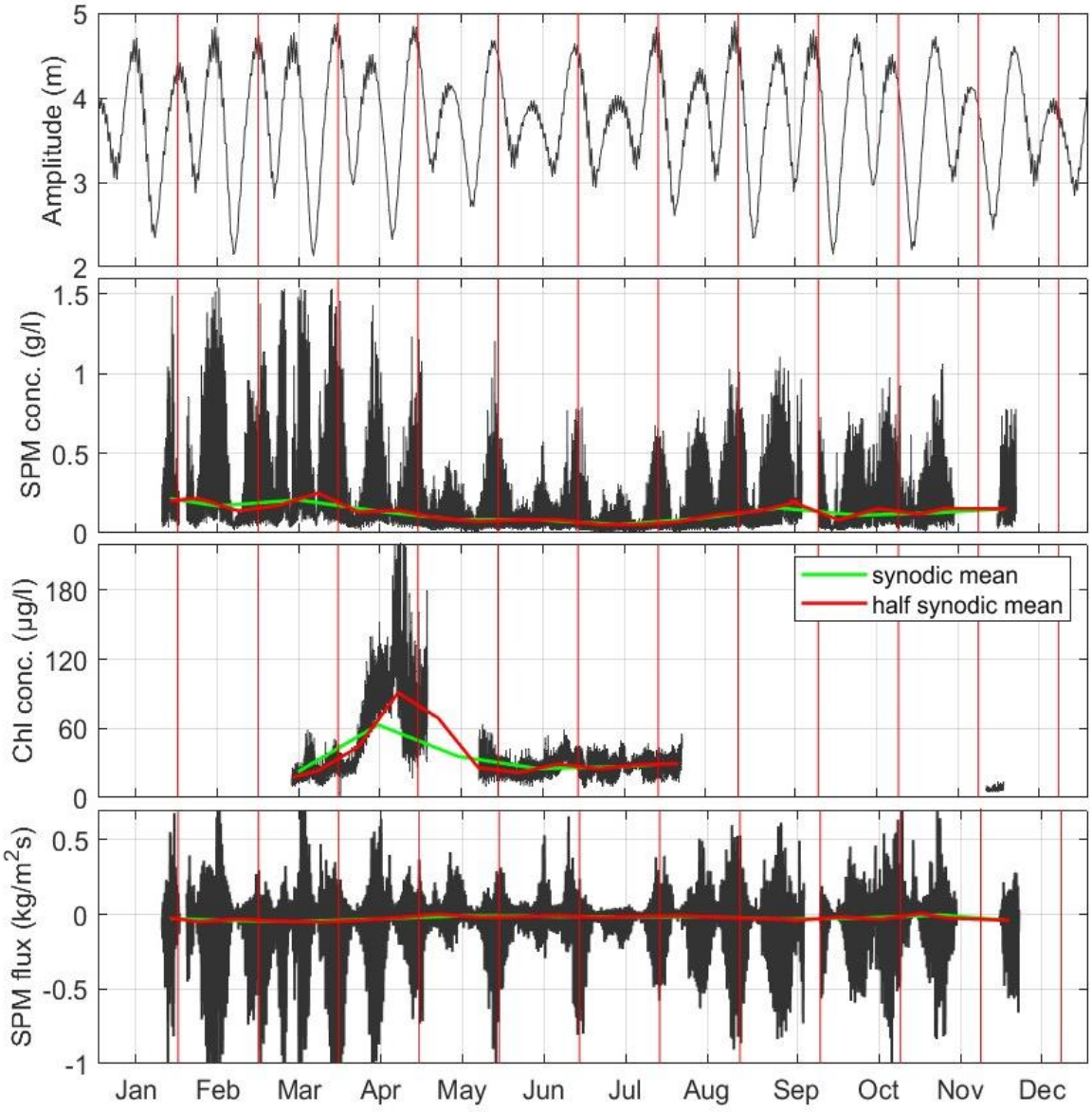

Figure 2.1: Tidal amplitude, SPM concentration, Chl concentration and SPM flux in 2013 at 2 m above the bed at MOW1. The red vertical lines indicate synodic periods. Further are shown the SPM and Chl concentrations, and SPM flux mean and over synodic and half synodic periods.

2.1.2. Simulation experiments with sampling schemes

Our approach simulated a number of in-situ water sampling schemes by picking and choosing data from the high-frequency time series according to in-situ monitoring programs with monthly or two-weekly sampling occasions and earth reconnaissance satellite programs with daily overflight repetitions (e.g. Timmerman, 2014; Herman et al., 2018; Azcarate et al., 2021; Fettweis et al., 2022). In total, ten different sampling schemes with varying sampling frequency have been implemented (Table 2.1). The six in situ random schemes can be divided into synodic (Synodic) and half-synodic (Hsynodic) depending on the time between two successive sampling events. For these random schemes (Synodic-1 to -3 and Hsynodic-1 to -3) the date and time of the sampling is selected by a random number generator.

Table 2.1: Sampling schemes used in the analysis.

Sampling scheme		Frequency	Tidal cycle	Number of samples
Random "in situ"	Synodic_1	29.5 days	1	13
	Synodic_2	29.5 days	0.5	6
	Synodic_3	29.5 days	-	1
	Hsynodic_1	14.7 days	1	13
	Hsynodic_2	14.7 days	0.5	6
	Hsynodic_3	14.7 days	-	1
Satellite	Synodic_ideal	29.5 days	-	30
	Hsynodic_ideal	14.7 days	-	15
	Synodic_realistic	29.5 days	-	1-12
	Hsynodic_realistic	14.7 days	-	1-7

Secondly, we considered four non-random schemes with regularly-spaced sampling events to simulate the one-pixel time-series as collected by polar orbiting earth reconnaissance satellites (e.g. MODIS-AQUA, MERIS, Sentinel-3/OLCI). The total number of satellite samples is on average 92 per year over the period 1998-2020 for the considered location. The mean amount of data at station MOW1 varies seasonally and equals one in December and January, and up to twelve in the summer months. The satellite sampling schemes are divided into an ideal and a realistic one. In the ideal satellite scheme, the sample is taken daily at noon, simulating a cloud-free situation. In the realistic satellite scheme, the sample is also taken at noon, while cloud cover and solar inclination angle are considered with the consequence that the number of data available is reduced.

The total number of samples per year taken by the random schemes Synodic-1 and Hsynodic-1 amounts to 156 and 286 (corresponding to 13 hourly samples during a tidal cycle for each of the 12 synodic or 22 half-synodic period) respectively, and 72 and 132 (corresponding to 6 hourly samples during half a tidal cycle for each of the 12 synodic or 22 half-synodic period) for the random schemes Synodic-2 and Hsynodic-2. For the Synodic-3 and Hsynodic-3 the total number of samples equals 12 and 22, respectively. The synodic and half-synodic random sampling schemes 1 and 2 resolve the quarter-diurnal and/or semidiurnal tidal variabilities, while random schemes 3 and the satellite sampling schemes do not.

To quantify the degree of information loss of the reduced sampling schemes, we computed a number of monitoring key quantities, i.e., half-synodic, synodic and annual means for both the constructed reduced-sample and the high-frequency MOW1 data time-series. We assumed the high-frequency means to represent the "true" values with no error and quantified the information loss of discrete low-frequency sampling by the differences between the "true" means and the "discrete sampling" means in probabilities due to the standard deviations of the latter. These standard deviations were computed for each sampling scheme (except for the ideal satellite schemes) by a bootstrap method with 1000 iterations with randomly altered sampling times to quantify the standard deviations of the annual, synodic and half-synodic means. The number of data available for the random sampling scheme varies between 1416 (half-synodic) and 2832 (synodic period). For the real

satellite sampling schemes this number is 15 and 30, as the random selection only picks up the day in the period, while the time is always at noon.

To test if interannual trends can be detected from the data extracted by the sampling schemes, time series of 20 years of SPM concentration or turbidity were constructed based on the concatenation of 20 times the MOW1 or the West Gabbard time series. The first year is the original time series, the successive years each have a 0.5% higher SPM concentration or turbidity than the previous year. The mean SPM concentration or turbidity in year 20 is thus about 10% higher than from the original time series. The satellite schemes cannot be applied to such a time series as they would pick every year values at the same moments of the tide, which is not realistic. Therefore, the satellite sampling schemes were adopted for the trend analysis such that a time was randomly chosen for every year; all the data selected during this year have the same time. The trend was calculated by a linear regression. The slope of the regression gives the trend while the p value provides its statistical significance, which is set as $P<0.05$.

2.2. Results

2.2.1. Periodic and annual mean derived from sampling schemes

As a first step we compared the half-synodic (Figure 2.2) and synodic means (Figure 2.3) computed for the high-frequency continuous data series and from the 1000 bootstrap subsampling of the above listed sampling schemes. The means of the 1000 bootstrap samplings are obviously close to the true means for all sampling schemes except for the satellite schemes in winter. However, the magnitudes of their standard deviations demonstrate the strong sensitivity of the individual means to altered picking times within each scheme. The magnitude of the standard deviations is determined by the number of samples involved and the variation in the high-frequency data. They are largest for the random sampling schemes 3 and lowest for the random sampling schemes 1 and show seasonal variations. For SPM concentration and flux, they are higher in winter than in summer, as SPM concentration shows higher variability in winter. For Chl concentration the standard deviations are highest in spring when the value changes fast during the spring bloom. The realistic satellite sampling schemes have more samples in spring and summer than in winter. Therefore, the satellite sampling in winter shows results closer to the random synodic and half-synodic sampling schemes-3. In contrast, in spring and summer, the standard deviation of the realistic satellite sampling scheme gets closer to the ones of the random schemes 1 and 2. This is because the number of data in the realistic satellite schemes is closer to the number of data in random schemes 1 and 2 depending on the satellite sampling considered (i.e., synodic or half-synodic).The standard deviation for the ideal satellite schemes is low during summer and slightly larger during winter for SPM concentration, while for Chl concentration highest standard deviations are occurring in spring.

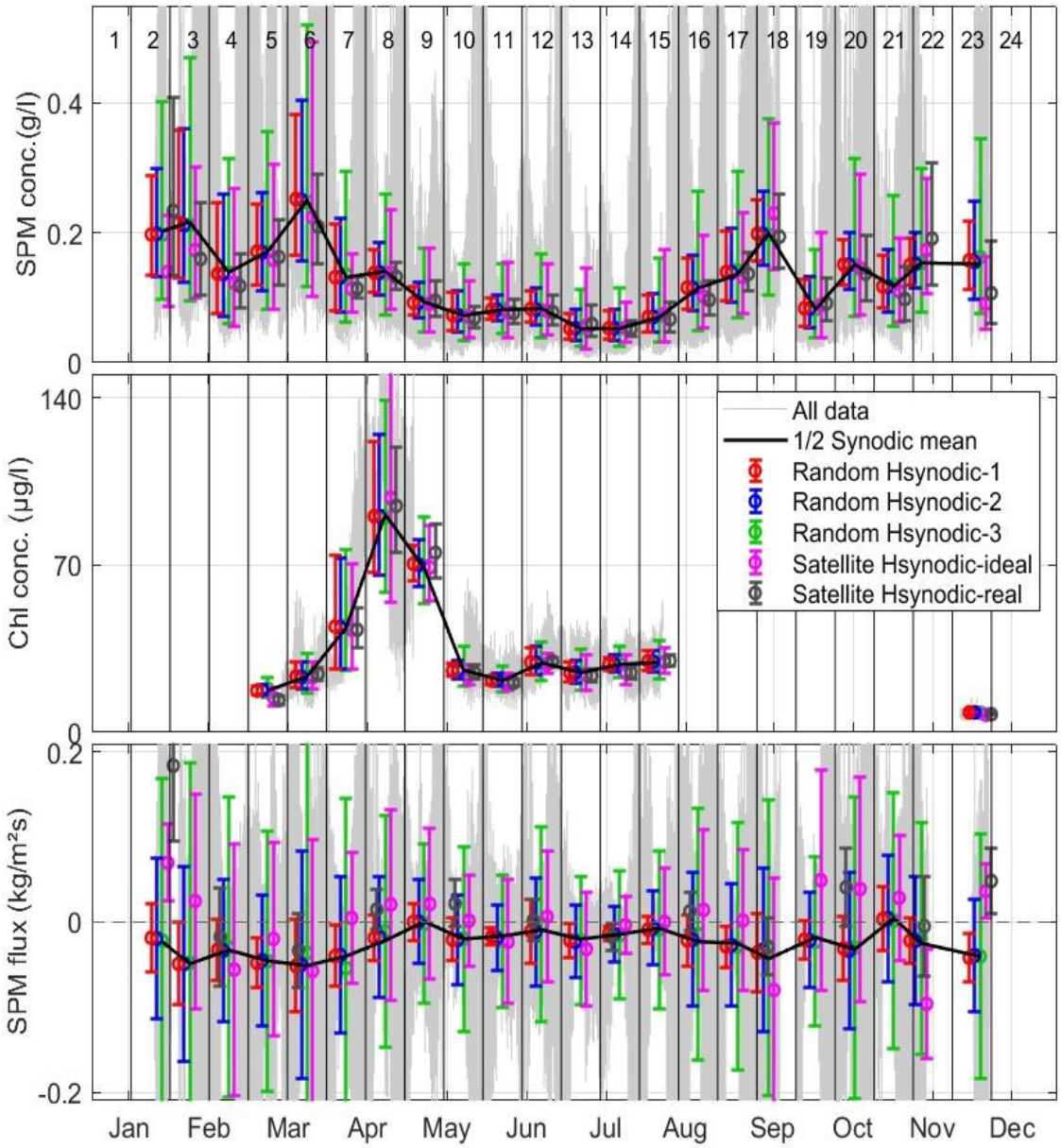

Figure 2.2: True half synodic mean SPM and Chl concentrations and SPM fluxes (black line) together with corresponding means from the random and satellite half synodic sampling scheme at MOW1. The error bars display the standard deviations (see text) for the random and the satellite schemes.

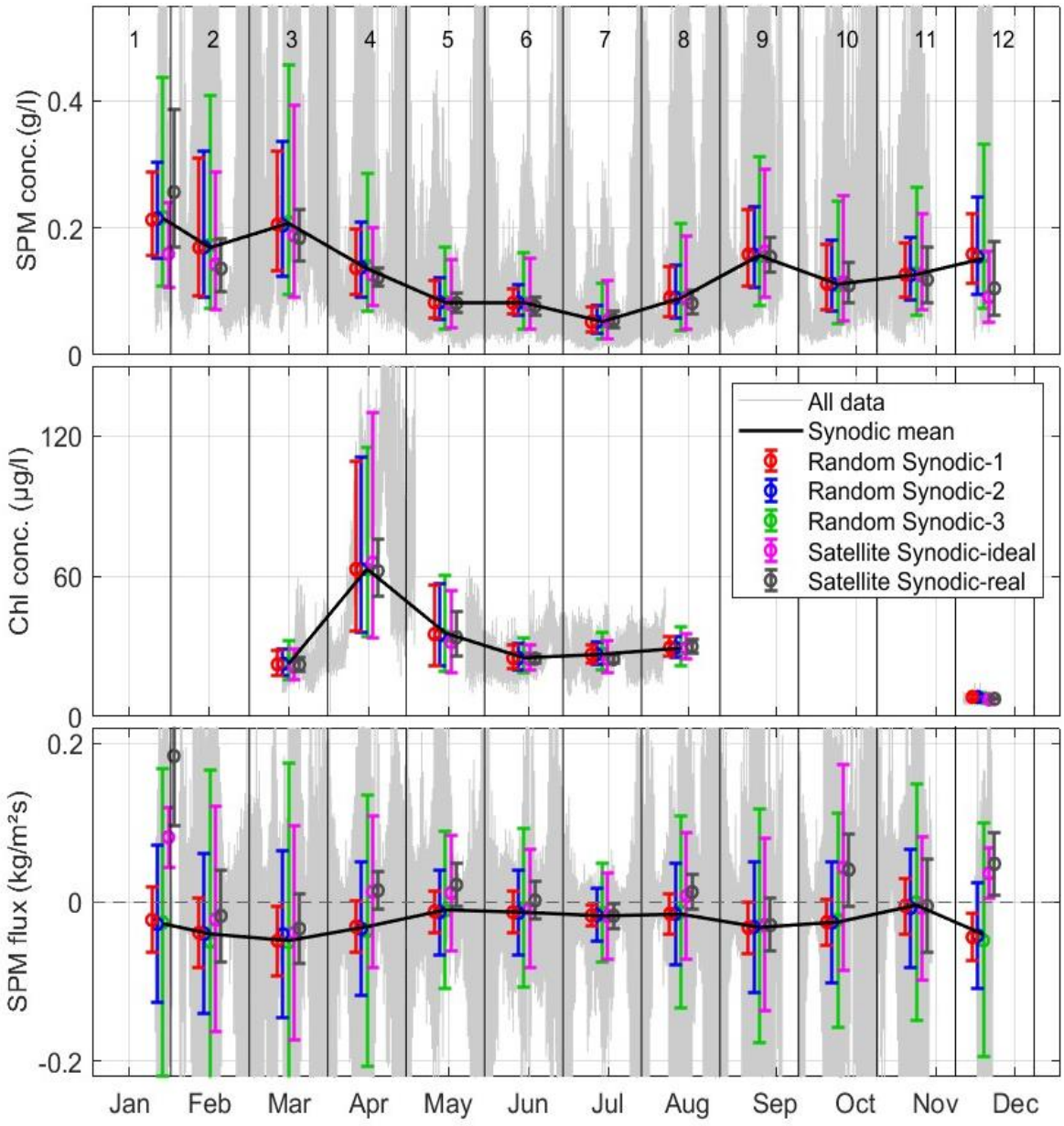

Figure 2.3: The same as Figure 2.2, but here for the synodic sampling period.

2.2.2. Accuracy of the mean SPM concentration, SPM flux and Chl concentration

The annual mean for the station MOW1 has been calculated for SPM concentration by taking the mean of all synodic or half-synodic periods. This is considered as the true annual mean and equals 132 mg/l for the synodic and 130 mg/l for the half-synodic mean. The annual mean and the standard deviation derived from the sampling schemes using a bootstrap method is shown in Table 2.2 together with the probability that the true mean is obtained within a certain margin (for example ± 2.5%, 5%, 10% and 33%). The results indicate that the probability of each scheme to match the true mean with statistical significance (<±2.5%) is low. The probabilities are similar for the random sampling schemes 1 (tidal cycle) and 2 (half a tidal cycle) but lower for scheme 3 (one sample). The satellite sampling schemes underestimate the true mean, an effect that is specific to polar-orbiting satellites that sample all individual stages of the semidiurnal and fortnightly harmonic

components, but not all combinations of the two due to tidal aliasing (Eleveld et al., 2014).

The probability of a sampling scheme to match the true mean depends on the season. Concerning SPM concentration, it is up to about 50% higher in summer than in the other seasons. The lower probabilities in winter, spring and autumn are caused by the higher variability and reinforced for the realistic satellite sampling schemes by the low number of satellite data during winter and autumn. In contrast to SPM concentration, Chl exhibits substantial changes in concentration in spring and summer due to primary production and grazing. The seasonal changes in Chl concentration respond to changes in drivers such as temperature or nutrient concentration. The probability of a sampling scheme to match the true mean Chl concentration is lowest during these periods. During spring, the half-synodic sampling scheme performs better than the synodic one. The probability that the true mean (34 µg/l over the synodic and 37 µg/l over the half-synodic periods) over the period March till August is obtained within a certain margin is shown in Table 2.3. Similar as for SPM concentration, the results indicate that the probability of each scheme to match the true mean with statistical significance (<±2.5%) is low. However, the half-synodic schemes have up to 100% higher probabilities during the period considered, which is dominated by the spring phytoplankton bloom.

The probabilities of matching the true mean SPM flux are low for all sampling schemes. Only random scheme 1 is able to estimate most of the time the direction of the residual flux correctly within one standard deviation. All the other schemes exhibit large uncertainties.

2.2.3. Interannual trends at MOW1 and West Gabbard

The trend over the re-built 20-year time series of SPM concentration at MOW1 has a true slope of 1.9×10^{-3} (mg/l day, $p\cong0$). The random and satellite sampling schemes have been applied as described in section 2.1.2. A linear regression was fitted through all data points obtained over the 20-year data series. A bootstrap method (number of iterations was 1000) was applied to obtain a 2D frequency distribution of slope and P values for all sampling schemes. The probability of detecting a positive and significant trend is presented in Table 2.4, together with the corresponding mean slope value. The results at MOW1 show low probabilities for all sampling schemes. The satellite sampling schemes perform less good than the random ones, which is caused by the unequal distribution of the data points over the year. Reducing the number of samples to half a tidal cycle or just one sample per period decreases the probability of finding a significant regression. For random sampling scheme 3, probabilities are lower than 6%. The histograms of slope versus P values is shown for MOW1 in Figure 2.4. By reducing the number of samples in the random schemes, not only the probability to obtain a positive trend gets less significant, but also the probability to find a reverse slope increases from 14% for the synodic (6% for half-synodic) sampling schemes 1 to 35% (resp. 29%) for sampling schemes 3.

To check whether these results are also valid for more offshore stations showing lower SPM concentrations, the same method was applied onto the 2010 turbidity time series from West Gabbard surface buoy. The true trend over the 20-year turbidity time series has a slope of 0.68×10^{-4} (FTU/day, $p\cong0$). The probability of detecting a positive and significant trend is also presented in Table 2.4 for West Gabbard, together with the mean slope value. The results show that the probabilities of finding the trend are significantly higher than at MOW1 but remain as low as at MOW1 for the random sampling scheme 3. The probability of finding a reverse slope at West Gabbard is below 7% for all sampling schemes.

Moreover, the slope is overestimated in all random and satellite sampling schemes by a factor 2 up to 7 at MOW1, and by a factor 3 up to 8 at West Gabbard. This suggests that when the sampling scheme reproduces a detectable trend its slope is often particularly pronounced. In contrast, when the sampling scheme leads to data with a weak slope (closer

to the true slope in this case), the variability in the randomly sampled values may mask the trend and prevent its detection with statistical significance (P<0.05).

Table 2.2: Probability (in %) of the sampling schemes to reproduce the true annual mean SPM concentration at MOW1 within ±2.5%, ±5%, ±10% and ±33%. The mean of 1000 samplings (in mg/l) is given together with the multiplicative standard deviation.

Sampling scheme		SPM conc.	±2.5%	±5%	±10%	±33%
Random	Synodic-1	132*/1.47	5	11	20	61
	Synodic-2	133*/1.54	5	10	18	56
	Synodic-3	132*/2.12	3	6	11	35
	½ Synodic-1	130*/1.43	6	11	22	66
	½ Synodic-2	130*/1.50	5	10	19	60
	½ Synodic-3	131*/2.10	3	5	11	36
Satellite	Synodic-ideal	118	-	-	-	-
	Synodic-real	124*/1.32	7	15	28	78
	½ Synodic-ideal	120	-	-	-	-
	½ Synodic-real	121*/1.40	6	11	23	69

Table 2.3: Probability (in %) of the sampling schemes to reproduce the true mean Chl concentration over the period March till August at MOW1 within ±2.5%, ±5%, ±10% and ±33%. The mean of 1000 samplings (in µg/l) is given together with the multiplicative standard deviation.

Sampling scheme		Chl conc.	±2.5%	±5%	±10%	±33%
Random	Synodic-1	34*/1.35	7	13	26	74
	Synodic-2	34*/1.37	6	12	25	72
	Synodic-3	34*/1.49	5	10	20	61
	½ Synodic-1	37*/1.21	10	21	40	91
	½ Synodic-2	37*/1.23	9	19	37	88
	½ Synodic-3	37*/1.38	6	12	24	70
Satellite	Synodic-ideal	33	-	-	-	-
	Synodic-real	33*/1.16	13	26	50	97
	½ Synodic-ideal	36	-	-	-	-
	½ Synodic-real	37*/1.13	16	32	59	99

Table 2.4: Probability of detecting a positive and significant (P<0.05) trend in a 20-year time series of SPM concentration at MOW1 and turbidity at West Gabbard. The mean slope for MOW1 (in mg/l day) and for West Gabbard (in FTU/day) is shown between brackets. The probability and mean slope value are calculated for all data and nine sampling schemes.

	MOW1		West Gabbard	
	Synodic	½ Synodic	Synodic	½ Synodic
All data	100% (1.9×10^{-3})		100% (0.68×10^{-4})	
random-1	46% (5.1×10^{-3})	61% (4.0×10^{-3})	85% (2.7×10^{-4})	87% (1.8×10^{-4})
random-2	26% (6.3×10^{-3})	39% (4.6×10^{-3})	73% (2.9×10^{-4})	78% (2.0×10^{-4})
random-3	4% (13.7×10^{-3})	6% (10.0×10^{-3})	17% (4.7×10^{-4})	12% (3.2×10^{-4})
Satellite-ideal	58% (3.1×10^{-3})		77% (1.0×10^{-4})	
Satellite-real	29% (5.5×10^{-3})	31% (5.5×10^{-3})	64% (1.9×10^{-4})	44% (1.7×10^{-4})

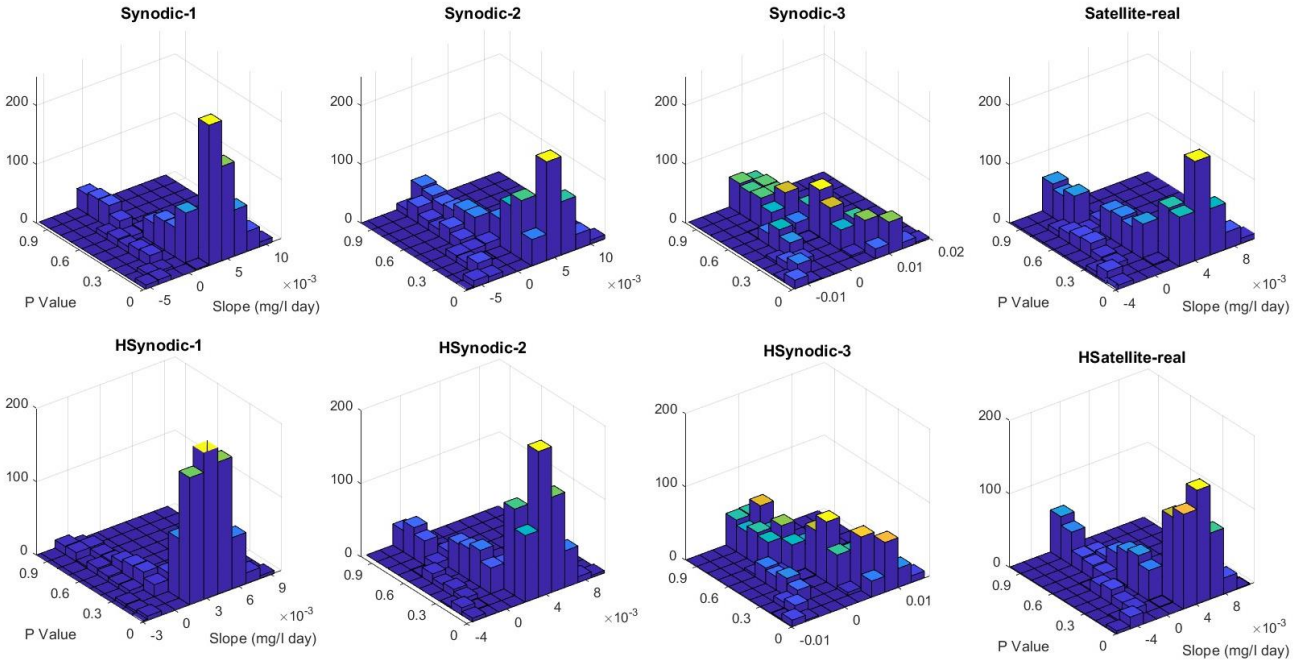

Figure 2.4: Trends in 20 year SPM concentration time series at MOW1 (every year SPM concentration increases by 0.5%). The histograms show the slope of the trends (true slope is 1.9×10^{-3} mg/l day) and the P values obtained by a bootstrap method for the eight sampling schemes. The z-axis is the number of iterations (in total=1000).

2.3. Discussions

Ideally monitoring should resolve all relevant temporal and vertical and horizontal spatial scales. In this study we have focused on the temporal scales by applying typical in situ and remote sensing sampling schemes to continuous time series of SPM and Chl concentration and SPM flux from a dynamic coastal area in order to evaluate the capacity of monitoring programs to resolve temporal scales. Do typical monitoring sampling schemes yield sufficient information to reach the goals of the programs, such as interannual trend detection? In the southern Bight of the North Sea and many other coastal areas, for

example, the SPM and Chl concentrations decrease from the coast towards offshore. In the same manner the variability in concentration decreases from the coast towards the offshore (Fettweis et al., 2022). These features, together with the temporal variations that are caused by tides, spring-neap cycles, seasons, and storms, define the monitoring efforts needed. Picking samples from a continuous time series leads to loss of information and this loss gets worse when the sampling intervals increase or when the main variabilities are not sampled. The frequency of the sampling determines the highest frequency about which we can get meaningful information from a set of data. In the case of tidal signals there are several frequencies that interfere. The highest frequencies are quarter- and semidiurnal and thus only the random sampling schemes 1 and 2 can provide information about them. The next lower ones are the half-synodic and the synodic frequencies. These schemes can only provide information on phenomena with periods longer than twice the sampling frequency. This means that the proposed sampling schemes cannot resolve neap-spring variability, but they can provide information on seasonal variations.

2.3.1. Detecting interannual trends with discrete sampling

Human activities (coastal management, dredged sediment disposal, sand mining, port developments, beach nourishments, bottom trawling, de-eutrophication, aquaculture) and climate change are changing or expected to change the SPM or Chl concentration at the time and space scales of these pressures. If these changes are small compared to the amplitudes of undisturbed natural variabilities, such as is the case for temporal trends related to global warming, coastal management or de-eutrophication, a consistent, long data record has to be available to detect their impacts (Henson et al., 2010; Fettweis et al., 2016; Desmit et al., 2020). Can synodic, half-synodic or satellite sampling schemes be used to detect interannual trends?

The results indicate that none of the sampling schemes can be used to assess statistically significant interannual trends with probabilities higher than 61% in a coastal turbidity maximum with large natural variability in SPM and Chl concentration such as at MOW1. The probabilities at West Gabbard are higher and the random sampling schemes 1 and 2 detect significant trends with a probability of up to 87% but remain low for the random sampling scheme 3. Further, in case a statistically significant trend was obtained, all sampling schemes overestimate the slope of the trend by a factor ranging from 2 to 8 at both sites.

How pronounced has a trend to be so that the sampling schemes can detect it with a high probability and with the correct trend value. Figure 2.5 shows the probabilities of the eight sampling schemes to detect a trend within ±25% of the correct trend value at the turbid station MOW1. The results indicate that the yearly increase has to be between 1 and 2% in order to obtain a probability of more than 60% for random sampling schemes 1 and 2 and for the satellite sampling schemes. Random sampling schemes 3 will detect trends with similar probability if the yearly increase is between 3 and 4%. These results imply that high-frequency time series are needed in coastal waters to resolve vertical (resuspension-deposition) and horizontal (transport) variations and to detect statistically significant ($P<0.05$) interannual trends and the increase/decrease of the interannual changes. Similar conclusions were formulated by Blauw et al. (2012) for phytoplankton monitoring in dynamic coastal areas.

How sound are interannual trend estimates derived from patchy time series? Gohin et al. (2019) detected trends in Chl concentration in the English Channel over six yearly averaged data when only the growth period (March-October) was considered, however, these authors increased the number of data points by applying a kriging interpolation technique to create daily values out of the spatial and temporal patchy satellite data. Capuzzo et al. (2015) have divided the North Sea into five hydrodynamic regions. For the

region that includes the high turbidity area along the Belgian-Dutch coastline, no significant trend has been found in SPM concentration over a period of 20 years, in contrast with offshore regions with lower turbidity or regions with long-term high-frequent time series such as in the East Anglia plume region. Similar results were found by Desmit et al. (2020) who only found significant trends in Chl concentration in stations with low turbidity values, but for example not in the Belgian nearshore area. OSPAR 2010 assessment combines the monitoring programs from different countries into large-scale areas. They conclude that the different sampling strategies, sampling protocols and the spatial heterogeneity hampers comparability of the monitoring results and of the detection of interannual trends. These results confirm our conclusions that the sampling scheme needs to be adapted to the temporal variability of the parameters. They also underline that coastal zones are often under sampled, even though these land-sea transition zones are highly dynamic, very productive and exhibit large variability in organic and inorganic particles composition and concentration (Levin et al., 2001; Talley et al., 2003, Blauw et al., 2018, Fettweis et al., 2022).

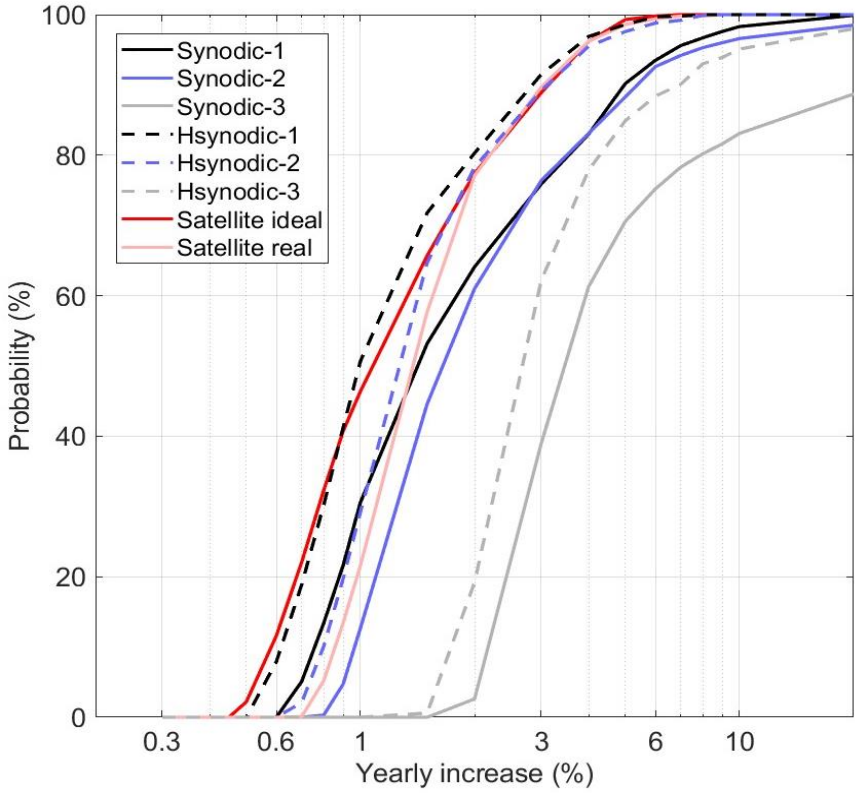

Figure 2.5: Probability of detecting a significant (p<0.05) and correct trend (within ±25% of the true value) with the different sampling scheme as a function of a given yearly increase in SPM concentration at MOW1.

2.3.2. What is the gain of using discrete sampling in a tidal system?

Are water samples of SPM and Chl concentration of any interest in a high turbid coastal area when sampled on a low frequency regarding tidal and neap-spring frequencies? If such sampling is the only form of monitoring, the interest is limited. A low frequency measurement will only detect if the water is turbid, oligotrophic, or eutrophic, a feature that could instead be easily derived from remote sensing products. However, when such sampling accompanies other forms of observation, they are of interest as they are needed to calibrate the sensors used in long-term continuous time series (e.g., turbidity, acoustic backscatter, fluorometer, remote sensing). As discussed above, continuous sensor

measurements provide periodic mean values with low uncertainty and a reliable determination of interannual trends. The relationship between sensor outputs (turbidity, acoustic backscatter or fluorescence) and the SPM or Chl concentration should be established using mass concentration derived from water samples (Roessler et al., 2017; Fettweis et al., 2019). Finally, low frequency samplings of SPM and Chl concentration are of interest when they can be combined with other water parameters sampled simultaneously, that escape detection by automated sensors or satellites. In the case SPM and Chl are correlated with other constituents (e.g., POC, PON, TEP), a sound analysis of the relationships between constituents can be made without necessarily resolving all variabilities. In recent analyses, Schartau et al. (2019) and Fettweis et al. (2022) have successfully modelled POC, PON and TEP concentrations from SPM concentrations along the coastal-offshore transect of eutrophic coastal zones with no special consideration for the tidal complexity of these parameters. SPM and Chl concentration can then be seen as indicator parameters as they are correlated or covarying with the concentration of these constituents.

2.3.3. True mean of SPM and Chl concentration and SPM flux

In our approach, the true mean over a specific period was derived from continuous sensor measurements. This mean value was considered "true" for the purpose of evaluating the performance of different sampling schemes. However, if our conclusion is using continuous sensors in turbid tidal systems, then we must ask how true is the "true" mean value? The drawback of sensor-derived continuous time series is that the quality or certainty of the data and thus any statistics based on it also depends on factors that are only to a certain level avoidable. Long-term observations of SPM and Chl concentration, for example, are the result of a complex ladder of operations that involve field, laboratory, and modelling methods (Roesler et al., 2017; Fettweis et al., 2019). Each step contributes its own random and systematic errors to the overall uncertainties of the sensor derived SPM or Chl concentration. Systematic errors related to the functioning of the sensors, the environment, the collection and processing of calibration samples and faulty human operations are detectable and sometimes correctable. If protocols for sample analysis and sensor calibration are carefully followed, uncertainties for SPM concentration can be confined within ±5%, otherwise they may reach up to ±20%. This means that a "true" mean, as assumed here, is always associated with an uncertainty that should be included in the analysis. Further the monitoring data are also associated with uncertainties that can reach up to 40% for satellite data (He et al., 2020; Wei et al., 2021) and up to a few percent for sample data (Fettweis et al., 2019).

2.4. Conclusion

The intent of our analysis was to provide researchers and policy makers with information on how to select appropriate sampling schemes depending on the variability of their system to derive meaningful results. This may help improve existing monitoring efforts. As our approach is system-dependent one should first quantify the variabilities in their area regarding the parameters they want to monitor, second specify the information they want to obtain (tidal, monthly, or annual mean, long term trends, calibration data...) and then define an appropriate monitoring scheme.

The effectiveness of different sampling schemes in resolving temporal variations relies on the sampling intervals and the number of samples taken per sampling occurrence. The analysis has shown that in highly turbid and dynamic coastal areas patchy time series obtained from low-frequency monitoring programs do not provide sufficient information to calculate mean values or interannual trends with statistical significance as they do not

resolve the main tidal variability. The performance of the sampling scheme is better at offshore sites, where the tidal dynamic is less important and the SPM and Chl concentration variabilities are lower. Still, when a significant ($p<0.05$) trend is detected in a randomly sampled data series in a high turbid coastal station, there is a 6 to 35 % probability that it is reversed compared to the "true" trend. If, however, the detected trend is correct its slope may be overestimated by a factor of 2 to 8 (whether inshore or offshore). Measurements taken at fixed times during a day, such as from satellites, introduce a bias in the data due to tidal aliasing, resulting in an underestimation of the mean concentrations.

In tidal turbid systems, SPM and Chl concentrations and SPM flux would better be monitored at high frequency using sensors to capture the full range of variabilities. This can be achieved by instrumented buoys or benthic landers who resolve variations related to tides, meteorological conditions, and seasons. However, sensor measurements do not yet offer the same guarantee of quality-assured data and in situ sampling remains needed for calibration. There is increasing evidence that climate change, eutrophication and de-eutrophication are altering the water quality and the underlying biogeochemical processes in coastal zones. Continuous sensor measurements may help detect and unravel these simultaneous decadal changes through the study of SPM and Chl long-term trends, with implications for the fate of coastal organic matter and the carbon cycle.

Still, it needs to be acknowledged that this work focuses on the temporal aspect of monitoring highly dynamic waters. Coastal systems are also often characterized by strong spatial gradients of Chl and SPM which would require an adequate distribution of in-situ stations to obtain a synoptic overview of the aquatic system which is often difficult or even impossible to maintain. Sampling a limited number of locations in a non-homogeneous area can result in a bias and over-representation of certain water types. In such areas the spatial coverage provided by satellite observations can support the continuous in-situ observations to provide a more representative assessment.

3. Referenties

Alvera-Azcarate A, Van der Zande D, Barth A, Troupin C, Martin S, Beckers J-M. 2021. Analysis of 23 years of daily cloud-free chlorophyll and suspended particulate matter in the Greater North Sea. Frontiers in Marine Science 13(19), 2657.

Anttila S, Ketola M, Vakkilainen K, Kairesalo T. 2012. Assessing temporal representativeness of water quality monitoring data. Journal of Environmental Monitoring 14, 589.

Blauw AN, Benincà E, Laane RWPM, Greenwood N, Huisman J. 2012. Dancing with the tides: Fluctuations of coastal phytoplankton orchestrated by different oscillatory modes of the tidal cycle. PLoS ONE 7(11): e49319.

Blauw AN, Benincà E, Laane RWPM, Greenwood N, Huisman J. 2018. Predictability and environmental drivers of chlorophyll fluctuations vary across different time scales and regions of the North Sea. Progress in Oceanography 161, 1-18.

Capuzzo E, Stephens D, Silva T, Barry J, Forster RM. 2015. Decrease in water clarity of the southern and central North Sea during the 20th century. Global Change Biology, 21, 2206–2214.

Conley, D., Paerl, H., Howarth, R., Boesch, D., Seitzinger, S., Havens, K., Lancelot, C., Likens, G., 2009. Controlling eutrophication: nitrogen and phosphorus. Science 323 (5917), 1014–1015. doi:10.1126/science.1167755

Desmit X, Nohe A, Borges AV, Prins T, De Cauwer K, Lagring R, Van der Zande D, Sabbe K. 2020. Changes in chlorophyll concentration and phenology in the North Sea in relation to de-eutrophication and sea surface warming. Limnology & Oceanography, 65, 828–847.

Druine F, Verney R, Deloffre J, Lemoine J-P, Chapalain M, Landemain V, Lafite R. 2018. In situ high frequency long term measurements of suspended sediment concentration in turbid estuarine system (Seine Estuary, France): optical turbidity sensors response to suspended sediment characteristics. Marine Geology 400, 24–37.

Eleveld MA, van der Wal D, van Kessel T. 2014. Estuarine suspended particulate matter concentrations from sun-synchronous satellite remote sensing: Tidal and meteorological effects and biases. Remote Sensing of Environment 143, 204-215.

Erkkilä A, Kalliola R. 2007. Spatial and temporal representativeness of water monitoring efforts in the Baltic Sea coast of SW Finland. Fennia - International Journal of Geography, 185, 107–132.

Fettweis M, Baeye, M, Cardoso C, Dujardin A, Lauwaerts B, Van den Eynde D, Van Hoestenberghe T, Vanlede J, Van Poucke L, Velez C, Martens C. 2016. The impact of disposal of fine grained sediments from maintenance dredging works on SPM concentration and fluid mud in and outside the harbor of Zeebrugge. Ocean Dynamics 66, 1497–1516.

Fettweis M, Riethmüller R, Verney R, Becker M, Backers J, Baeye M, Chapalain M, Claeys S, Claus J, Cox T, Deloffre J, Depreiter D, Druine F, Flöser G, Grünler S, Jourdin F, Lafite R, Nauw J, Nechad B, Röttgers R, Sotollichio A, Vanhaverbeke W, Vereecken H. 2019. Uncertainties associated with in situ long-term observations of suspended particulate matter concentration using optical and acoustic sensors. Progress in Oceanography, 178, 102162. doi:10.1016/j.pocean.2019.102162

Fettweis M, Schartau M, Desmit X, Lee BJ, Terseleer N, Van der Zande D, Parmentier K, Riethmüller R. 2022. Organic matter composition of biomineral flocs and its influence on suspended particulate matter dynamics along a nearshore to offshore transect. Journal of Geophysical Research: Biogeosciences, 127, e2021JG006332

He J, Chen Y, Wu J, Stow DA, Christakos G. 2020. Space-time chlorophyll-a retrieval in optically complex waters that accounts for remote sensing and modeling uncertainties and improves remote estimation accuracy. Water Research 171, 115403.

Henson SA, Sarmiento JL, Dunne JP, Bopp L, Lima I, Doney SC, John J, Beaulieu C. 2010. Detection of anthropogenic climate change in satellite records of ocean chlorophyll and productivity, Biogeosciences 7, 621–640.

Herman PMJ, van Kessel T, Vroom J, Dankers, P.J.T., Cleveringa, J., de Vries, B., Villars, N., 2018. Mud dynamics in the Wadden Sea – Towards a conceptual model. Report 11202177-000-ZKS-0011, Deltares, The Netherlands.

Gaulier C, Zhou C, Guo W, Bratkič A, Superville P-J, Billon G, Baeyens W, Gao Y, 2019. Trace metal speciation in North Sea coastal waters. Science of the Total Environment 692, 701-712.

Gohin F, Van der Zande D, Tilstone G, Eleveld MA, Lefebvre A, Andrieux-Loyer F, Blauw AN, Bryère P, Devreker D, Garnesson P, Hernández Fariñas T, Lamaury Y, Lampert L, Lavigne H, Menet-Nedelec F, Pardo S, Saulquin B. 2019. Twenty years of satellite and in situ observations of surface chlorophyll-a from the northern Bay of Biscay to the eastern English Channel. Is the water quality improving? Remote Sensing of Environment 233, 11134.

Grabemann I, Krause G. 1989. Transport processes of suspended matter derived from time series in a tidal estuary. Journal of Geophysical Research 94 (C10), 14373–14379.

Harvey ET, Kratzer S, Philipson P. 2015. Satellite-based water quality monitoring for improved spatial and temporal retrieval of chlorophyll-a in coastal waters. Remote Sensing of Environment 158, 417–430.

Keil RG, Montiuçon DB, Prahl FG, Hedges JI. 1994. Sorptive preservation of labile organic matter in marine sediments. Nature 370, 549–552.

Kirby MF, Law RJ., 2010. Accidental spills at sea – Risk, impact, mitigation and the need for co-ordinated post-incident monitoring. Marine Pollution Bulletin 60, 797-803.

Kowalska M, Güler H, Cocke DL. 1994. Interactions of clay minerals with organic pollutants. Science of the Total Environment 14, 223-240.

Lauwaert B, Fettweis M, De Witte B, Van Hoei G, Timmermans S, Hermans L. 2019. Vooruitgangsrapport (juni 2019) over de effecten op het mariene milieu van baggerspeciestortingen (Vergunningsperiode 01/01/2017 – 31/12/2021). RBINS-ILVO-AMT-CD rapport. BL/2019/01, 28pp.

Lauwaert B, De Witte B, Festjens F, Fettweis M, Hermans L, Lesuisse A, Le H-M, Seghers S, Timmermans S, Vanavermaete D, Van Hoey G. 2021. Synthesis report on the effects of dredged material dumping on the marine environment (licensing period 2017-2021). RBINS-ILVO-AMT-AMCS-FHR report BL/2021/10, 67pp.

Levin LA, Boesch DF, Covich A, Dahm C, Erséus C, Ewel KC, Kneib RT, Moldenke, A, Palmer MA, Snelgrove P, Strayer D, Weslawski JM. 2003. The function of marine critical transition zones and the importance of sediment biodiversity. Ecosystems 4, 430-451.

Lin H, Yu Q, Wang Y, Gao S. 2022. Identification, extraction and interpretation of multi-period variations of coastal suspended sediment concentration based on unevenly spaced observations. Marine Geology 445, 106732.

Lovett GM, Burns DA, Jenkins JT, Mitchell MJ, Rustad L, Shanley JB, Likens GE, Haeuber R. 2007. Who needs environmental monitoring? Frontiers in Ecology and the Environment 5, 253-260.

Mack L, Attila J, Aylagas E, Beermann A, Borja A, Hering D, Kahlert M, Leese F, Lenz R, Lehtiniemi M, Liess A, Lips U, Mattila O-P, Meissner K, Pyhälahti T, Setälä O, Strehse JS, Uusitalo L, Willstrand WA, Birk S. 2020. A Synthesis of marine monitoring methods with the potential to enhance the status assessment of the Baltic Sea. Frontiers in Marine Science 7.

Ransom B, Kim D, Kastner M, Wainwright S. 1994. Organic matter preservation on continental slopes: Importance of mineralogy and surface area. Geochimica et Cosmochimica Acta 62, 1329-1345.

Roesler C, Uitz J, Claustre H, Boss E, Xing X, Organelli E, Briggs N, Bricaud A, Schmechtig C, Poteau A, D'Ortenzio F, Ras J, Drapeau S, Haëntjens N, Barbieux M. 2017.Recommendations for obtaining unbiased chlorophyll estimates from in situ chlorophyll fluorometers: A global analysis of WET Labs ECO sensors. Limnology and Oceanography Methods 15, 572–585.

Schartau M, Riethmüller R, Flöser G, van Beusekom JEE, Krasemann H, Hofmeister R, Wirtz K. 2019. On the separation between inorganic and organic fractions of suspended matter in a marine coastal environment. Progress in Oceanography 171, 231–250.

Sea-Bird Electronics, 2011. Calculating Calibration Coefficients for WET Labs ECO-AFL and ECO-FL Fluorometer, ECO-NTU Turbidity Meter, and ECO-FL-NTU Fluorometer/Turbidity Meter. APPLICATION NOTE NO. 62

Talley DM, North EW, Juhl AR, Timothy DA, Conde D, de Brouwer JFC, Brown CA, Campbell

LM, Garstecki T, Hall CJ, Meysman FJR, Nemerson DM, Souza Filho PW, Wood RJ. 2003. Research challenges at the land–sea interface. Estuarine, Coastal and Shelf Science 58, 699-702.

Timmerman JG. 2014. Information Needs for Water Management. CRC Press, Taylor & Francis Group, 208pp.

Wei J, Wang M, Jiang L, Yu X, Mikelsons K, Shen F. 2021. Global Estimation of Suspended Particulate Matter From Satellite Ocean Color Imagery. Journal of Geophysical Research Oceans 126(8), e2021JC017303.

Wernand MR. 2010. On the history of the Secchi disk. Journal of the European Optical Society - Rapid Publications 5, 10013s.

COLOPHON

Dit rapport werd voorbereid door de BMM in maart 2023
Zijn referentiecode is MOMO/10/MF/202303/NL/AR/2

De scheepstijd met de RV Belgica werd voorzien door BELSPO en KBIN-OD Natuur

Indien u vragen hebt of bijkomende copies van dit document wenst te verkrijgen, gelieve een e-mail te zenden naar mfettweis@naturalsciences.be, met vermelding van de referentie, of te schrijven naar:

Koninklijk Belgisch Instituut voor Natuurwetenschappen
OD Natuur – BMM
t.a.v. Michael Fettweis
Vautierstraat 29
B–1000 Brussel
België
Tel: +32 2 627 41 83

BEHEERSEENHEID VAN HET
MATHEMATISCH MODEL VAN DE NOORDZEE

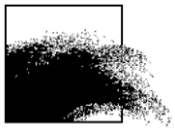

APPENDIX 1

Ho NQ, Fettweis M, Hur J, Desmit X, Kim JI, Jung DW, Lee SD, Lee S, Choi YY, Lee BJ. 2022. Flocculation kinetics and mechanisms of microalgae- and clay-containing suspension in different microalgae growth phases. Water Research 226, 119300

Water Research 226 (2022) 119300

Contents lists available at ScienceDirect

Water Research

journal homepage: www.elsevier.com/locate/watres

Flocculation kinetics and mechanisms of microalgae- and clay-containing suspensions in different microalgal growth phases

Que Nguyen Ho [a,b], Michael Fettweis [c], Jin Hur [d], Xavier Desmit [c], Jae In Kim [a], Dae Won Jung [e], Sang Deuk Lee [e], Sungyun Lee [a,f], Yun Young Choi [a], Byung Joon Lee [a,f,*]

[a] Energy Environment Institute, Kyungpook National University, 2559 Gyeongsang-daero, Sangju, Gyeongbuk 37224, South Korea
[b] Faculty of Environment and Labour Safety, Ton Duc Thang University, Ho Chi Minh City, Viet Nam
[c] Operational Directorate Natural Environment, Royal Belgian Institute of Natural Sciences, Rue Vautier 29, Bruxelles B-1000, Belgium
[d] Department of Environment & Energy, Sejong University, Seoul 05006, South Korea
[e] Nakdonggang National Institute of Biological Resources (NNIBR), Sangju, Gyeongsangbuk-do 37242, South Korea
[f] Department of Advanced Science and Technology Convergence, Kyungpook National University, 2559 Gyeongsang-daero, Sangju, Gyeongbuk 37224, South Korea

ARTICLE INFO

Keywords:
Flocculation
Microalgae
Clay
Floc size distribution
Bayesian calibration

ABSTRACT

Interplays between microalgae and clay minerals enhance biologically mediated flocculation, thereby affecting the sedimentation and transportation of suspended particulate matter (SPM) in water and benthic environments. This interaction forms larger flocs with a higher settling velocity and enhances SPM sinking. The aim of this study was to investigate the flocculation kinetics of microalgae and clay in suspension and to elucidate the mechanisms associated with such interactions. Standard jar test experiments were conducted using various mixtures of kaolinite and microalgal samples from batch cultures (*Chlorella vulgaris*) to estimate biologically mediated flocculation kinetics. The organic matter (OM) composition secreted by the microalgae was characterized using a liquid chromatography - organic carbon detection system, and quantitative analysis of transparent exopolymer particles was conducted separately. A two-class flocculation kinetic model, based on the interaction between flocculi and flocs, was also adopted to quantitatively analyze the experimental data from flocculation. Results from the flocculation kinetic tests and OM analyses, in association with other data analyses (i.e., floc size distribution and flocculation kinetic model), showed that flocculation increased with OM concentration during the growth phase (10–20 d). However, on day 23 during the early stationary phase, flocculation kinetics started decreasing and substantially declined on day 30, even though the amount of OM (mainly biopolymers) continued to increase. Our results indicate that an adequate quantity of biopolymers produced by the microalgal cells in the growth phase enhanced floc-to-floc attachment and hence flocculation kinetics. In contrast, an excessive quantity of biopolymers and humic substances in the stationary phase enhanced the formation of polymeric backbone structures and flocculation via scavenging particles but simultaneously increased steric stabilization with the production of a large number of fragmented particles.

1. Introduction

Flocculation is a complex physicochemical process involving the aggregation and breakage of suspended particulate matter (SPM) in water environments. Aggregation induces floc formation from mineral and organic particles, while breakage disaggregates large flocs into smaller flocs or primary particles (Lee et al., 2012a; Maggi, 2005). The flocculation rate depends on SPM concentration, turbulence, and the presence of organic matter in the water column, among other ambient conditions (Mietta et al., 2009; Winterwerp, 1998). Flocculation determines the structure, density, and settling velocity of flocs, and thus, the overall fate of the SPM. Therefore, flocculation also affects SPM

Abbreviations: AB, alcian blue; DI, deionized; DOC, dissolved organic carbon; DOM, dissolved organic matter; DW, dry weight; EPSs, extracellular polymeric substances; FA, fulvic acid; FSD, floc size distribution; HS, humic substances; LC-OCD, liquid chromatography - organic carbon detector; LMW, low molecular weight; OCD, organic carbon detector; UVD, ultraviolet detector; OD, optical density; OM, organic matter; PSD, particle size distribution; SPM, suspended particulate matter; TCPBE, two-class population balance equation; TEP, transparent exopolymer particles; XG, xanthan gum.

* Corresponding author.
E-mail address: bjlee@knu.ac.kr (B.J. Lee).

https://doi.org/10.1016/j.watres.2022.119300
Received 18 April 2022; Received in revised form 15 October 2022; Accepted 24 October 2022
Available online 26 October 2022

transport in many practical applications (e.g., siltation of navigation channels, pollutant and nutrient transport, and geomorphological evolution) (Maggi, 2009).

Climate change, population increase, industrialization, and agribusiness development are serious stressors of aquatic systems. These stressors contribute to excess nutrients (i.e., nitrogen and phosphorous) and clay minerals from various point and nonpoint sources discharging into aquatic environments, which creates favorable conditions for eutrophication (Preisner et al., 2021). The resulting eutrophication causes intense algal blooms worldwide and turbid waters (Diaz and Rosenberg, 2008). In addition to long-term trends imposed by land use and climate change, a modification in flocculation patterns may alter SPM dynamics and budgets in pelagic and benthic systems, thereby potentially influencing the carbon cycle (Engel et al., 2004). It has become clear that microalgae may interact with clay to enhance flocculation (Neumann et al., 2019). Such biologically mediated flocculation is expected to affect hydrological, biochemical, and ecological fluxes in aquatic environments. Understanding the interactions between microalgae and clay minerals may eventually lead to innovative solutions for the management of freshwater, estuaries, and coastal systems.

Clay minerals, which have cohesive properties (Manning et al., 2011), participate in flocculation and are a major component of flocs in aquatic environments (Spencer et al., 2021). The most abundant clay minerals (e.g., chlorite, montmorillonite, kaolinite, and illite) in aquatic environments are sourced from the crust of the Earth surface (Sionneau et al., 2008). These minerals are eroded by rainfall, river flow, melting ice, or wind, and are eventually discharged into aquatic environments (Fagel, 2007). Their cohesive properties result from attractive physicochemical forces (i.e., van der Waals and electrostatic forces). They are tightly bound in small, dense flocculi (a word composed of flocs and nuclei) through electrostatic attraction. Flocculi may further aggregate to form large, fluffy flocs through the gluing action of extracellular polymeric substances (EPSs) and mucus produced by microalgae (Partheniades, 2009). This stepwise growth from clay minerals to flocculi and then to flocs tends to accelerate under aggregation-favorable conditions with a high clay concentration and moderate turbulence (Partheniades, 2009). The interactive processes between flocculi and flocs are characterized by the bimodality of the particle/floc size distribution (Lee et al., 2012a) and are mathematically formulated as a two-class population flocculation kinetic model (Lee et al., 2011).

The presence of microalgae promotes aggregation of SPM in aquatic environments because microalgae can secrete substantial amounts of dissolved, sticky polysaccharides (EPSs), some of which are precursors to transparent exopolymer particles (TEP) (Xiao and Zheng, 2016). The highest concentrations of EPS are usually associated with microalgal blooms (Passow, 2002). Highly viscous and sticky EPSs can facilitate flocculation by combining many components, including solid, non-sticky particles; cells; detritus; and dissolved substances (Chin et al., 1998; Passow, 2002; Villacorte et al., 2009; Walch et al., 2022). Clay and microalgae are abundant fine particles prevalent in many water and benthic environments (Dallmann et al., 2020; Drummond et al., 2014). Therefore, they are commonly found in floc structures and govern the fate and transportation of SPM in aquatic environments.

Clay and microalgae interact with each other and control flocculation and transportation, mediating biological and physicochemical processes in aquatic environments. Avnimelech and coworkers demonstrated that if the clay content is sufficiently high, microalgae will form flocs with clay particles and sink to the bottom, enhancing the clarity of water (Avnimelech and Menzel, 1984; Avnimelech et al., 1982). The aggregation of microalgae and clay increases the settling velocity of the resulting flocs, thereby removing SPM, detritus, and microalgae from the water column to the bed layer (Avnimelech et al., 1982). Verspagen et al. (2006) depicted the flocculation of clay and buoyant cyanobacteria and the sedimentation of biomineral flocs. Biologically mediated flocculation has been often reported to enhances sedimentation in microalgal- and clay-containing suspensions (Deng, 2022; Deng et al., 2019; Fettweis et al., 2022; Liu et al., 2016). Kiørboe et al. (1990, 1994) determined if a specific microalgae type or species was responsible for this phenomenon through *in-situ* observations that diatoms could aggregate with clay minerals and form large biomineral flocs in the Danish Ise Fjord. Similarly, de Lucas Pardo et al. (2015) investigated the flocculation potential between cohesive sediment and different species of *Cyanobacteria* and found that *Aphanotece* yielded larger biomineral flocs in microalgal- and clay-containing suspensions than *Aphanizomenon* did. However, the detailed mechanisms of biogeochemical flocculation mediated by microalgae and clay minerals are highly complex and remain poorly understood in pelagic and benthic systems. Therefore, more attention and efforts are necessary to investigate the mechanisms and kinetics of the interaction between microalgae and clay and the resulting flocculation.

Clay minerals or composites (e.g., montmorillonite, kaolinite, local red soil, and chitosan-clay composites) can be utilized for the removal and harvesting of harmful microalgae via biologically mediated flocculation. The interaction between microalgae and clay enhances the formation of large biomineral flocs with densities higher than that of water, resulting in the removal of buoyant microalgae from water bodies (Kim et al., 2016; Nakayama et al., 2004; Sengco and Anderson, 2004; Shemesh et al., 2021; Verspagen et al., 2006; Wei et al., 2020; Yin et al., 2022). For instance, Wei et al. (2020) applied montmorillonite modified cationic starch to enhance sedimentation of *Chlorella vulgaris*, which increased the settling velocity of the formed biomineral flocs by 2.34-fold. Clay-modified cation starch has also been applied to enhance the removal of other microalgae species, such as *Microcystis aeruginosa* (Shi et al., 2016). Shemesh et al. (2021) used iron-coated clays (i.e., red clays) to promote the formation of biomineral flocs and increase the sedimentation and removal of *Cyanobacteria*. This produced large biomineral flocs with a mean size of 600 μm and a 73% higher sedimentation rate (Shemesh et al., 2021). Thus, biologically mediated flocculation of microalgae and clay minerals is beneficial for controlling algal blooms or the removal and harvesting of microalgae in water bodies and mass-production systems.

Previous studies have demonstrated the occurrence and practical use of biologically mediated flocculation of microalgae and clays under specific conditions. However, the mechanism and kinetics of biologically mediated flocculation in continuum of the microbial population and biochemical dynamics remained unknown. Therefore, this study aimed to investigate the mechanism and kinetics of the biochemical flocculation, by maintaining a well-controlled microalgae batch culture and performing flocculation kinetic tests with microalgae- and clay-containing suspensions in different phases of microalgal growth. To the best of our knowledge, little or no consideration has been given to the role of OM (more specifically EPS and humic substances) on flocculation kinetics in batch cultures during the growth phase of microalgae. In this study, we monitored the microalgal growth phase and organic matter composition of a microalgal batch culture. We investigated their effects on flocculation kinetics and the mechanisms occurring in microalgae- and clay-containing suspensions. In addition, a flocculation kinetic model and Bayesian calibration were applied to estimate the flocculation kinetics of microalgae- and clay-containing suspensions at various microalgae growth phases. The findings of this study on biologically mediated flocculation may eventually help to predict the fate and transport of SPM in coupled pelagic-benthic systems, enhance microalgae removal in water bodies, and improve harvest in mass-production systems in the future.

2. Materials and methods

2.1. Microalgal culture

C. vulgaris is a well-characterized species of microalgae that is often involved in algal blooms (Jacquet et al., 2005). *C. vulgaris* is also known to release sticky biopolymers (i.e., EPS) (Babiak and Krzemińska, 2021);

hence, it was selected as a model species to investigate flocculation kinetics and mechanisms in microalgae- and clay-containing suspensions. *C. vulgaris* was provided by the Nakdonggang National Institute of Biological Resources (NNIBR, Sangju, Korea). Cultivation of microalgae was performed in a 5 L bioreactor with Bold's basal medium (Sigma-Aldrich, USA). The temperature and light intensity of the bioreactor were maintained at room temperature (20 ± 2°C) and 3000 LUX, respectively. The microalgae bioreactor was sealed with a glass fiber filter (GF-C 1.2 μm) (HYUNDAI Micro, Korea) to prevent contamination and gently stirred to minimize the formation of microalgal aggregates and precipitates.

Microalgal samples were regularly collected from the bioreactor to perform flocculation kinetic tests. In each sample, the microalgal biomass weight was measured as the retained dry weight (DW) (Chioccioli et al., 2014) on a glass filter (GF-C 1.2 μm, HYUNDAI micro, Korea) after drying the sample at temperature 105°C for 2 h (US Environmental Protection Agency, 2001). The optical density at 600 nm (OD_{600}) was measured by DR 3900 (HACH, USA) as an indicator of the microbial growth state (600 nm light source minimizes unexpected cell damage and growth) (Stevenson et al., 2016).

2.2. Flocculation kinetic test

Flocculation kinetic tests were performed by mixing a microalgae sample with a clay-containing suspension in a standard 2 L jar tester (Phipps and Bird, USA) (Fig. 1). Kaolinite purchased from Sigma-Aldrich (St. Louis, USA) was used as a model clay for the flocculation kinetic tests (particle size was 0.1–4 μm). Right before the flocculation kinetic test, 10 mL from the kaolinite stock solution (10 g/L) was added to 2 L of deionized water (DI) to produce a final kaolinite concentration of 0.05 g/L in the test jar.

The ionic strength and pH of the suspension were adjusted to 0.01 mol/L NaCl and pH 7, respectively. After adding 10 mL of the microalgal sample to the suspension, the microalgae- and kaolinite-containing suspension was homogenized with rapid mixing at 200 rpm ($g \approx 250/s$) for 10 min and gently stirred at 80 rpm ($g \approx 85/s$) afterwards, until the change in floc size reached equilibrium. The suspension was continuously delivered from the test jar to a LISST-200X particle size analyzer (Sequoia Scientific Inc., Bellevue, USA) through a 6 mm diameter tube using a peristaltic pump at a flow rate of 100 mL/min (Mietta et al., 2009). The LISST-200X instrument monitored the change in floc size distribution (FSD) during the test period, and the FSD data collected from the instrument were used for further analysis of flocculation kinetics.

2.3. Decomposition of the subordinate peaks of a floc size distribution

The FSD of a microalgae- and clay-containing suspensions is generally multimodal with superposition of subordinate lognormal FSDs because of hierarchical floc formation with mineralogical and biological components (Lee et al., 2012a). The FSDs in this study mostly displayed multimodal peaks and were subjected to further numerical analysis of the FSD peak decomposition. Multimodal FSDs were assumed to be formed by the overlapping of three unimodal log-normal PSDs of primary particles, flocculi, and flocs (Fig. 2) (Lee et al., 2012a; Van Leussen, 1994).

These FSD data were input to the in-house computer program, which performed the curve fitting analysis and decomposition of the observed FSD into subordinate log-normal FSDs (Eq. (1)) (Hussein, 2005; Whitby, 1967).

$$\frac{dV}{dD} = \sum_{i=1}^{3} \frac{V_i}{\sqrt{2\pi}\ln(\sigma_i)} exp\left[\frac{-1}{2}\left(\frac{ln(D/D_{mean,i})}{ln(\sigma_i)}\right)^2\right] \quad (1)$$

where the subscript i denotes primary particles, flocculi, or flocs; D is the diameter of each size class of the measured FSD; $D_{mean,i}$ is the geometric mean diameter for a lognormal distribution (Weisstein, 2001); σ_i is the geometric standard deviation; and Vi is the volumetric concentration of the i-th unimodal FSD. Nine parameters for $D_{mean,i}$, σ_i, and Vi of primary

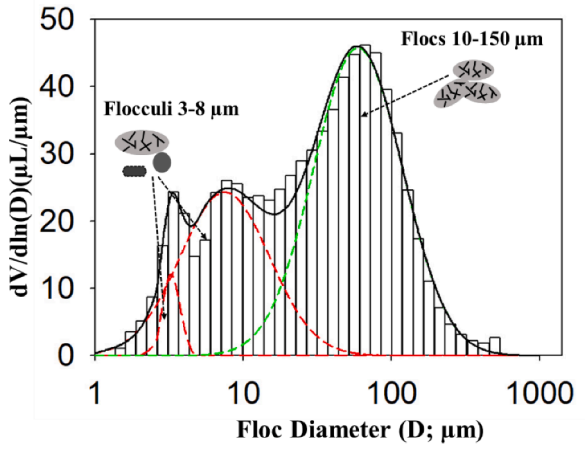

Fig. 2. A multimodal particle size distribution and schematic diagram of the discrete aggregate groups of flocculi (including primary particles) and flocs.

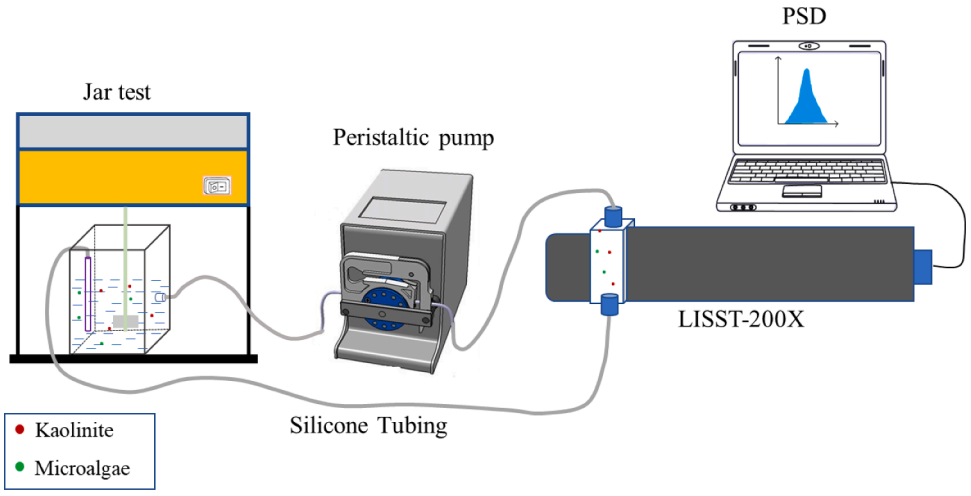

Fig. 1. Schematic diagram illustrating the experimental setup for the flocculation test of microalgae (i.e., *Chlorella vulgaris*) and the clay-containing suspension. PSD, particle size distribution.

particles, flocculi, and flocs were estimated, and the best-quality PSD was found at the minimum error between the simulated and measured FSDs (Hussein, 2005; Whitby, 1967).

2.4. Estimation of the settling velocity of flocs

The settling velocity (w_s) of flocs was estimated as a proxy for the sedimentation and removal rate of FSD containing various size classes of biomineral flocs, based on the modified Stokes equation with floc fractal dimensions (Winterwerp, 1998). The mean settling velocity was calculated by dividing the sum of the mass-weighted settling velocity of each size class by the total mass of the FSD (Lee et al., 2012a).

$$w_s = \sum_i \frac{m_i}{m_T}\left(\frac{1}{18}\frac{(\rho_s-\rho_w)}{\mu} g D_p^{3-n_f}\frac{D_i^{n_f-1}}{1+0.15Re_i^{0.687}}\right) \quad (2)$$

In Eq. (2), m_i is the mass of each size class of FSD obtained from the LISST instrument. Total mass of the FSD is represented by m_T. Densities of primary particles and water are denoted by ρ_s and ρ_w, respectively, and were fixed at 2600 and 1000 kg/m^3, respectively. Based on observations, the size of primary particles (D_p) was set at 2.5 μm. The fluid viscosity (μ) and gravitational acceleration (g) were 0.001 kg/m.s and 9.81 m/s^2, respectively. D_i is the mean size of each size class of the FSD. In accordance with earlier studies, the fractal dimension (n_f) was fixed at 2. Reynolds number, Re_i, depicts each size class (Lee et al., 2012a).

2.5. Characterization of OM composition

2.5.1. Liquid chromatography - organic carbon detector (LC-OCD)

An LC-OCD system (DOC Labor Dr. Huber, Karlsruhe, Germany) was used to characterize the dissolved OM (DOM) composition in the microalgal samples with respect to the molecular size distribution. This system involves chromatographic columns with organic carbon and ultraviolet (UV) detectors (OCD and UVD). A mobile phase including phosphate buffer of pH 6.85 was used, and the flow rate was maintained at 1.1 mL/min. An aliquot (1 mL) of the sample was injected into the instrument and filtered through a 0.45 μm in-line polyethersulfone filter (Sartorius, Germany) prior to chromatographic separation and detection for dissolved organic carbon (DOC) and UV absorbance at 254 nm. For molecular mass calibration, Suwannee River humic acid (SRHA) and fulvic acid (SRFA) were obtained from the International Humic Substances Society (IHSS) (Huber et al., 2011). An in-house software package (ChromCALC LC-OCD systems; DOC-Labor GmbH) was used to acquire and process the chromatographic data and quantify different size fractions. This software package classifies the OM composition based on the molecularity and aromaticity, including biopolymers (MW > 20,000 Da), humic substances (HS) (1,000 < MW < 20,000 Da), building blocks (300 < MW < 500 Da), and low molecular weight (LMW) neutrals and acids (MW < 350 Da).

2.5.2. Transparent exopolymer particle (TEP) measurement

The TEP concentration was measured using the analytical method of Passow and Alldredge, and Nosaka (Nosaka et al., 2017; Passow and Alldredge, 1995) as an indicator of bio-polymeric substances (EPS). A sample from the microalgal bioreactor was filtered through a Whatman 0.45 μm Nucleopore filter (Sigma-Aldrich, USA), and the TEPs on the filter were stained with Alcian Blue (Sigma-Aldrich, USA). The filter was then rinsed with DI water and stored in Petri dishes at − 20°C. On the day of the chemical analysis, the stored filter papers were transferred from Petri dishes to brown bottles of concentrated (80%) sulfuric acid, and the bottles were then shaken on an orbital table shaker (DAIHAN, Korea). The amount of Alcian Blue (AB) released from the TEPs on a filter paper was quantified using a DR 3900 HACH spectrophotometer (HACH, USA), in terms of absorption at 787 nm. The stained particles were related to an anion density weight equivalent to that of TEP and were standardized using xanthan gum (mg XG/L). Xantham gum (XG) has been widely used as a proxy for TEP because of its polysaccharidic structure and presence of reactive anionic groups for AB staining and better replicability (Passow and Alldredge, 1995; Villacorte et al., 2015). The standard curve consisted of a series of known amounts of xanthan gum (Sigma-Aldrich, USA). The detailed procedures for creating a standard curve can be found in earlier studies, which are shown in the supplementary document.

2.6. Flocculation kinetic model and parameter estimation

2.6.1. Flocculation kinetic model: two-class population balance equation

A flocculation kinetic model and Bayesian calibration were applied to evaluate the flocculation kinetics of microalgae- and clay-containing suspensions in each flocculation kinetic test. Because the FSDs, formed by biologically mediated flocculation in water and benthic environments, have been mostly recognized to be bimodal with flocculi and flocs fractions (Fettweis and Baeye, 2015), we adopted a two-class population balance equation (TCPBE) that consists of size-fixed flocculi and size-varying flocs (Lee et al., 2011). The TCPBE incorporates three coupled differential equations describing the time rate of change in the concentration of flocculi = dN_P/dt (Eq. (3)), the concentration of flocs (dN_F/dt) (Eq. (4)) and the total concentration of flocculi bound to flocs (dN_T/dt)($N_T = N_C \times N_F$) (Eq. (5)).

The number of flocculi bound in a floc (N_C) was used as an index of floc size in the TCPBE. The aggregation and breakage kernels for the collision frequency factor (β) and breakage kinetic function (a) were formulated using the shear- and size-dependent breakage kinetics functions (Eqs. (6) and (7)) (Burd and Jackson, 2002; Lee et al., 2011). Lee et al. (2011) explained TCPBE in depth.

$$\frac{dN_P}{dt} = -\frac{1}{2}\alpha_{PP}\beta_{PP}N_PN_P\left(\frac{N_C}{N_C-1}\right) - \alpha_{PF}\beta_{PF}N_PN_F + fN_Ca_FN_F \quad (3)$$

$$\frac{dN_F}{dt} = \frac{1}{2}\alpha_{PP}\beta_{PP}N_PN_P\left(\frac{1}{N_C-1}\right) - \frac{1}{2}\alpha_{FF}\beta_{FF}N_FN_F + a_FN_F \quad (4)$$

$$\frac{dN_T}{dt} = \frac{1}{2}\alpha_{PP}\beta_{PP}N_PN_P\left(\frac{N_C}{N_C-1}\right) + \alpha_{PF}\beta_{PF}N_PN_F - fN_Ca_FN_F \quad (5)$$

$$\beta_{SH,ij} = \frac{1}{6}(D_i+D_j)^3G \quad (6)$$

$$a_F = E_bG\left(\frac{D_F-D_P}{D_P}\right)^p\left(\frac{\mu G}{F_y/D_F^2}\right)^q \quad (7)$$

In Eqs. (3)–(7), D_P and D_F indicate the mean diameters of the flocculi or flocs, respectively; f is the fraction of flocculi generated by the floc breakage; α_{PP}, α_{PF}, and α_{FF} indicate the collision efficiency factors for flocculi-flocculi, floc-floc, and flocculi-floc attachments, respectively; and the subscripts i and j of the collision frequency factor (β) indicate either flocculi (P) or flocs (F). The collision efficiency factor (α) is generally used as an application-specific fitting parameter. E_b is the efficiency of the breakage process, μ is the absolute viscosity of the fluid, G is the shear rate [s^{-1}], F_y is the yield strength of flocs, and p and q are the empirical parameters determined experimentally. Of the numerous parameters listed in Table 1, the collision efficiency factors (α_{PP}, α_{PF}, and α_{FF}), the empirical parameters of the breakage kinetic function (p and q), and the mass fraction of microflocs generated by the breakage of macroflocs (f) were selected as parameters to be estimated by Bayesian calibration. Each set of best-fit parameters in the flocculation kinetic test was used as an index to diagnose the flocculation kinetics of the microalgae- and clay-containing suspensions.

2.6.2. Bayesian calibration for parameter estimation

The notable stochastic calibration method is Bayesian inference, the purpose of which is to learn about unknowns, such as calibration parameters from measured or observed data (Gep and Tiao, 1973). The

Table 1
Model parameters used in the TCPBE flocculation kinetic model.

Classification	Symbol	Prior Distribution (Fixed Value)	Remark
Curve-fitting Parameters	α_{PP}	[0.0–1.0]	collision efficiency factors
	α_{PF}	[0.0–1.0]	α_{PP} is assumed the same as
	α_{FF}	[0.0–1.0]	α_{PF}.
	p	[0.01–1.5]	empirical parameters of
	q	[0.01–1.5]	breakage kinetics
	f	[0.0–1.0]	fraction of flocs produced by breakage
Fixed Parameters	E_b	2.0e-4	efficiency factor for floc breakage [$s^{0.5}$/m]
	F_y	1.0e-10	yield strength of flocs [Pa]
	μ	1.0e-6	absolute viscosity of the fluid [N·s/m^2]
	G	95	shear rate of the fluid [/s]
Initial Condition	$N_{T,0}$ / $N_{PT,0}$	0.01	initial mass fraction of flocs
	$D_{F,0}$	1.0e-5	concentration of macroflocs [/m^3]

Bayesian framework can infer a posterior distribution of unknowns based on the known data (Eq. (8)). This procedure of Bayesian calibration ensures that the nonlinear or linear relations are explained and the matching uncertainties are measured, both of which cannot be easily recognized manually (Beckers et al., 2020). Therefore, Bayesian calibration was applied to estimate the best-fit simulation and model parameters which were used to estimate the flocculation kinetics of the microalgae- and clay-containing suspensions in this study.

$$P(X \mid \tilde{y}) = P(X) \cdot L(X \mid \tilde{y}) \tag{8}$$

The differential evolution adaptive metropolis (DREAM) software package (Vrugt et al., 2009), which is based on a Bayesian inference, was used to estimate the best-fit model parameters for each flocculation kinetics test. The outcome of Bayesian calibration is the posterior probability distribution of the model parameters for the measurement data, reflecting the uncertainty of the different parameters. The posterior distribution is calculated from the prior distribution of the parameters (Table 1) and the likelihood function of the parameters considering the measured data (floc diameter, D_F; and flocs' volumetric fraction, V_F). The DREAM software package estimated not only the best-fit model parameters but also the posterior distribution of the model parameters. Vrugt et al. (2009) explained the DREAM algorithm and mathematical formulation in detail (Vrugt et al., 2009).

3. Results and discussion

3.1. Microalgal culture

The DW and OD_{600} of the microalgal suspension obtained from the bioreactor tended to increase during the incubation period, showing three typical phases: the initial lag, exponential growth, and stationary phases (Fig. 3). During the lag phase (0–8 d), increases in DW and OD_{600} were insignificant as DW increased to 30 mg/L and OD_{600} increased to 0.094. Afterwards, DW and OD_{600} increased substantially during the exponential growth phase (8–23 d), up to 756 mg/L and 1.7, respectively. The increase in DW and OD_{600} was mitigated during the stationary phase (23–30 d). Higher concentrations of microalgal cells, denoted by higher DW and OD_{600} during both the exponential growth and stationary phases, are expected to increase the chance of collision and attachment between cells and other particles (Giorgi et al., 2019; Tang, 2016). In addition, microalgae have been reported to produce a larger amount of sticky biopolymers (e.g., EPS), which enhance flocculation kinetics during the exponential growth and stationary phases (Nguyen et al., 2005; Villacorte, 2014). The effect of OM composition on flocculation kinetics will be discussed in later sections.

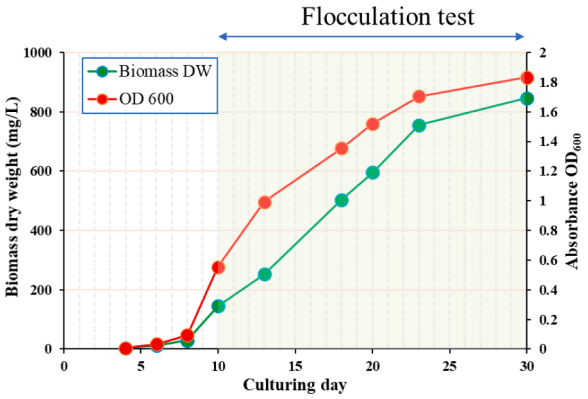

Fig. 3. Dry weight (DW) and optical density (OD_{600}) of the microalgae culture as a function of incubation time.

3.2. Organic matter composition in different microalgal growth phases

The TEP and DOC concentrations of the microalgal suspension obtained from the microalgal batch culture were monitored throughout the during the entire incubation period (Fig. 4a). The TEP concentration continuously increased from 0.4 to 57.0 mg/L, as the equivalent XG

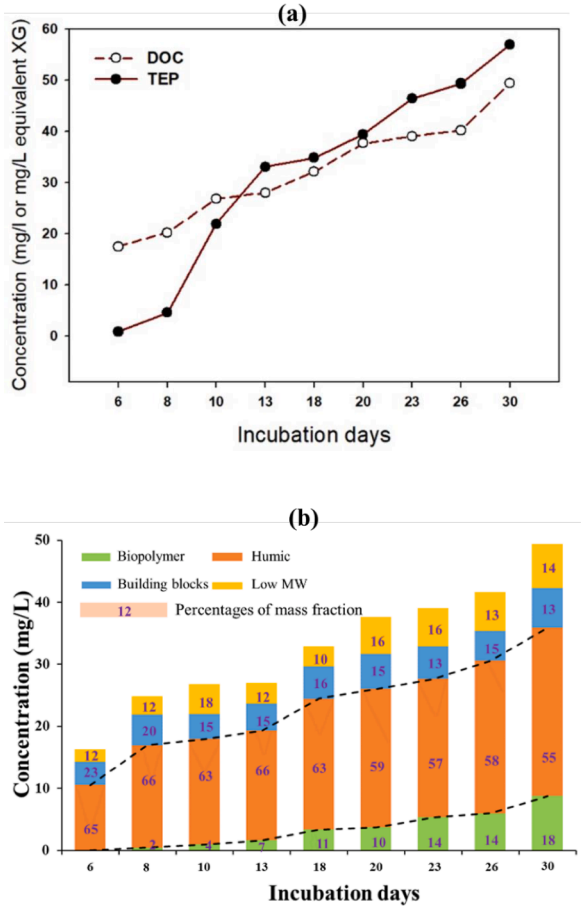

Fig. 4. (a) Dissolved organic carbon (DOC) and transparent exopolymer particles (TEP) concentration during the incubation period of the *Chlorella vulgaris* culture. The respective concentration units of DOC and TEP are mg/L as the organic carbon and mg/L as the equivalent xantham gum concentration. (b) The concentration and relative fraction of the organic matter components are biopolymers (MW > 20,000 Da), humic substances (1,000 < MW < 20,000 Da), building blocks (300 < MW < 500 Da), and low molecular weight substances (MW < 350 Da).

concentration increased, and the DOC concentration increased from 16.3 to 49.4 mg/L. During the growth phase, a DOC production rate was estimated at 0.18 mg/L/h, similar to the 0.24 mg/L/h of an earlier study (Nguyen et al., 2005). As the number of cells in the microalgal batch culture increases, extracellular organic carbon is generated and accumulates due to cell lysis and direct exudation (Ducklow, 1993; Nagata, 2000; Nguyen et al., 2005; Villacorte, 2014). Such release of extracellular organic carbon from healthy or stressed cells is a common physiological process of some phytoplankton species (Fogg, 1977; Sharp, 1977).

The change in the DOM fractions measured with the LC-OCD system indicated that the HS fraction decreased from 65 to 55% during the incubation period, but the HS concentration increased from 10.6 to 27.1 mg/L (Fig. 4b). The HS of the microalgal samples was characterized as aquagenic fulvic acid (FA), which is produced by aquagenic microorganisms, based on the measurement of its molecularity and aromaticity (Huber et al., 2011; Lee et al., 2017). In contrast, biopolymers were almost absent in the initial lag phase, but they increased gradually in the exponential growth and stationary phases, up to 8.8 mg/L concentration and 18% mass fraction out of the total DOC concentration (Fig. 4b). Because biopolymers are the precursors of sticky and aggregation-prone TEP, a higher concentration and fraction of biopolymers is supposed to enhance the flocculation potential of the algae- and clay-containing suspension (Villacorte, 2014).

3.3. Floc size distributions in the flocculation kinetic tests

Inspection of the FSDs of the microalgae- and clay-containing suspensions, obtained from the flocculation kinetic tests revealed that the FSDs were generally superimposed, with three distinct peaks of primary particles, flocculi, and flocs, in the respective size ranges of 1–2.5 μm, 3–8 μm, and 10–100 μm (Fig. 5). Based on the two-class flocculation theory [28], primary particles and flocculi form the building blocks of flocs, so that they are integrated into a single group of flocculi for data analysis and flocculation kinetic models (Alldredge and Silver, 1988; Lee et al., 2012a; Van Leussen, 1994). In each flocculation kinetic test, the size and volumetric fraction of flocs (i.e., the position and area of the peak) increased with time, whereas the volumetric fraction of flocculi decreased while maintaining a narrow size range (i.e., 1–8 μm). Higher concentrations of sticky biopolymers were expected to increase the size and volume of flocs (i.e., flocculation potential) through the inclusion of flocculi into the flocs.

The floc size and volumetric fraction reached equilibrium at the end of the flocculation kinetics test. The equilibrium floc size and volumetric

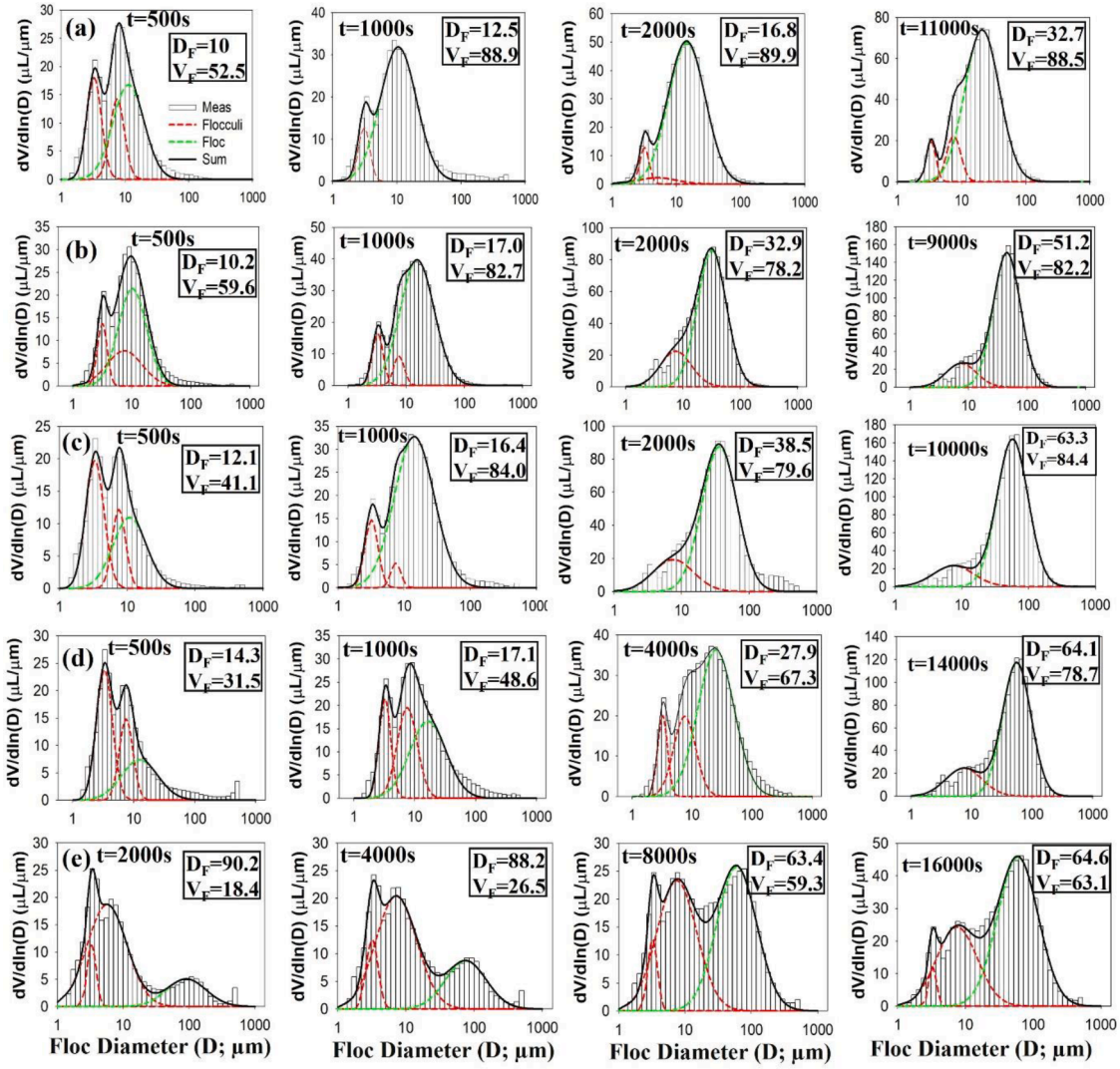

Fig. 5. (a), (b), (c), (d) and (e) are floc size distributions (FDS) obtained from the flocculation kinetic tests of the clay and microalgal suspensions after 10 d, 13 d, 20 d, 23 d, and 30 d of incubation time. Each figure represents the FSD measured by the LISST-200X particle size analyzer (Sequoia Scientific Inc., Bellevue, USA) at the time of the flocculation kinetic test. Flocs size (μm) and volumetric fraction (%) are denoted by D_F and V_F, respectively.

fraction, measured at the end of each flocculation test, gradually increased during the growth phase (10, 13, and 20 d) (see the last panels of Fig. 5a–c) but changed little in the stationary phase (23 and 30 d) (see the last panels of Fig. 5d, e). Notably, the FSDs at 30 d were different from those during the earlier days of incubation. The flocculation kinetics at 30 d was quick to develop an apparent peak of flocs at a very early time; there was a distinct peak of flocs of 90 μm and 18% volumetric fraction at 2000 s (see the first panel of Fig. 5e). The peak of flocs continued to increase its volumetric fraction from 18 to 63% while approaching the equilibrium state. However, a large fraction (37%) of flocculi (the peak at approximately 8 μm) remained intact and stabilized in the microalgae- and clay-containing suspensions at the equilibrium (see the last panel of Fig. 5e). This observation indicates that not all flocculi were subject to flocculation, but more remained present at 30 d than after shorter incubation periods.

3.4. Parameter estimation with the two-class flocculation kinetic model

Fig 6 shows the time series of the floc size (D_F) and the flocs' volumetric fraction (V_F) obtained from the flocculation kinetic tests at 10, 13, 18, 20, 23, and 30 d of microalgal incubation. The best-fit simulation was also indicated by $p < 0.05$. D_F at the equilibrium and the speed to reach equilibrium increased in the 10–20 d period and then started decreasing at 23 d (Fig. 6a). D_F at 30 d, did not show a clear trend in floc size growth, but flocs were scattered in the range of 50 to 90 μm (Fig. 6a). V_F at equilibrium and the speed to reach equilibrium were similar for the tests at 10, 13, 18, and 20 d (Fig. 6b). V_F reached equilibrium within 2000 s. However, V_F at equilibrium and the speed to reach equilibrium decreased in the 23–30 d period. In fact, the flocculation kinetics of the microalgae- and clay-containing suspensions increased as the microalgal incubation time increased but started decreasing at 23 d. This behavior of flocculation kinetics seems to correspond to the change in the OM composition in different microalgal growth phases (see Section 3.2).

The aggregation and breakage parameters were estimated using Bayesian calibration Fig. 7. These parameters clearly indicate a transition in flocculation kinetics from 23 d. The collision efficiency factors of flocculi and flocs (α_{PP} and α_{FF}, respectively), as the indices of flocculation potential, increased during the 10–13 d period, remained high in the 13–20 d period, and decreased in the 23–30 d period. The empirical breakage parameters (p, q) remained constant during the 10–20 d period. During the 23–30 d period, p decreased but q increased. This behavior of p and q indicates that the breakage of flocs become more

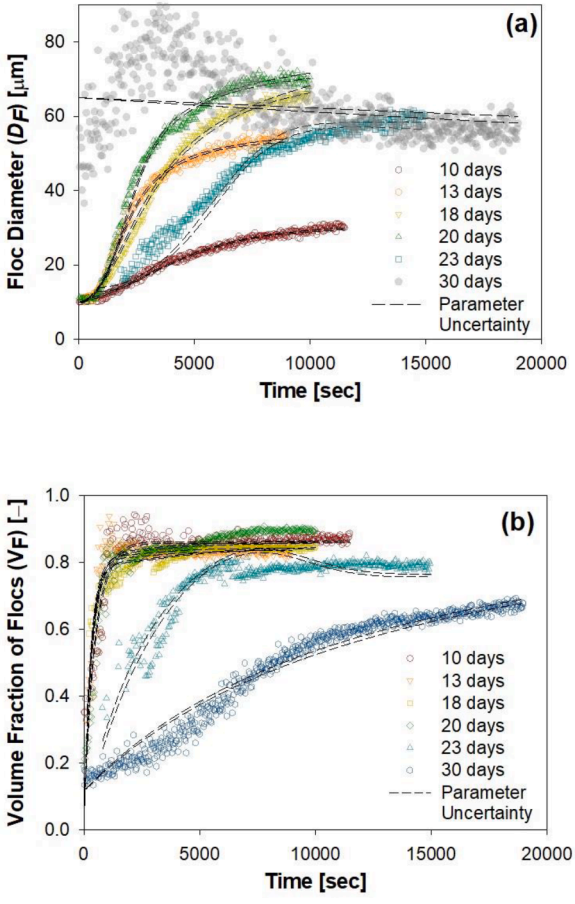

Fig. 6. Time series of (a) the floc diameter and (b) the flocs' volumetric fraction with 95% simulation uncertainty intervals due to parameter and total uncertainty, for the flocculation kinetic tests at 10, 13, 18, 20, 23, and 30 d of the microalgal incubation time.

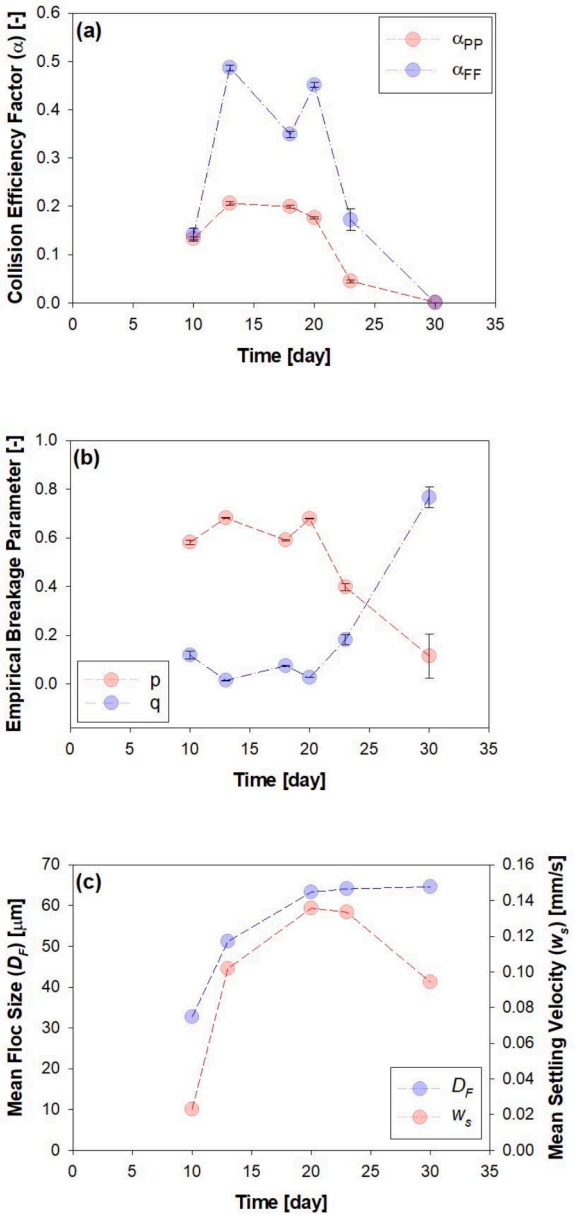

Fig. 7. Best-fit parameters of (a) collision efficiency factors (α_{PP} and α_{FF}) and (b) empirical breakage parameters (p and q) at 10, 13, 18, 20, 23, and 30 d of microalgal incubation. (c) The settling velocity and flocs size at the equilibrium of the flocculation kinetic tests as a function of the incubation period.

vulnerable to floc size (D_F) and shear rate (G), based on the mathematical formulae presented in Eqs. (3) to (7). In other words, flocs in the 23–30 d period were more fragile than those in the earlier period of the microalgal growth phase.

Fig. 7c illustrates the variation in the size and settling velocity of the biomineral flocs at the equilibrium of each flocculation kinetic test as a function of the incubation period. The floc size increased sharply at the beginning and reached a plateau; however, the settling velocity reached a peak and afterward decreased gradually. The floc size reached a plateau (63–65 μm) at day 20, whereas the settling velocity started to decrease at the same time. A further decrease of the settling velocity to 0.094 mm/s was observed at day 30. The remaining volume fraction of flocculi (rightmost images in Figs. 5c–e) was unsettled and reduced the overall settling velocity of the biomineral flocs in the batch. This result shows that to maximize microalgae removal or harvest, clay should be applied during the growth phase.

The results from the flocculation kinetic tests in the growth phase (10–20 d) indicated a typical flocculation mechanism based on floc-to-floc collision and attachment. Fig. 8 is an example of flocculation kinetics in the growth phase after 13 d of microalgal incubation time. Although the floc volumetric fraction (V_F) reached its maximum within 1000 s (Fig. 8b), the floc size (D_F) increased gradually and reached equilibrium in 8000 s (Fig. 8a). The respective peaks of flocculi and flocs in the best-fit simulation also matched those of the experimental data (Fig. 8c). It is important to note that D_F (i.e., the second peak) gradually increased from 10 μm at 500 s to 17 μm at 1000 s, 33 μm at 2000 s, and 45 μm at 4000 s. In other words, the peak of the flocs (i.e., the right peak in Fig. 8c) gradually moved from left to right. Continuous floc-to-floc aggregation might induce this gradual increase in D_F, in which flocs might collide and attach to each other and generate larger flocs in series (Fig. 10).

The flocculation kinetics of the microalgae- and clay-containing suspensions were found to change drastically during the stationary phase (i.e., 23–30 d). In particular, the flocculation kinetics at 30 d was unique, without indication of a gradual floc-size increase (Fig. 9). Large flocs (~90 μm) had already emerged at the beginning of the test with a substantial volumetric fraction (~18%), and afterwards, they maintained their large size in the range of 60 to 90 μm (Fig. 9a). The volumetric fraction of flocs (V_F) gradually increased and ended up at 63% at equilibrium, indicating that a substantial fraction of flocculi (37%) remained intact at equilibrium (Fig. 9b) (see also Fig. 5e). At 30 d of incubation, sturdy and shear-resistant microbial backbone structures appeared to exist initially, and they scavenged and trapped smaller flocculi in their backbone structures as time increased. Simultaneously, steric stabilization of flocculi caused by an excessive number of biopolymers and humic substances might also be a prominent reason for retaining a large amount (~37%) of intact flocculi at equilibrium.

3.5. Implications

A conceptual model is proposed to interpret flocculation and stabilization occurring in a microalgae and clay-containing suspension with respect to the microalgal growth phases (Fig. 10). This conceptual model suggests two distinct mechanisms for biologically mediated flocculation and stabilization. First, floc-to-floc collision and attachment might be the governing flocculation mechanism in the microalgal growth phase (i.e., flocculation kinetic tests at 10–20 d). An adequate quantity of biopolymers produced by the microalgal cells in the growth phase might enhance floc-to-floc collision and attachment (Avnimelech et al., 1982; Droppo, 2001) and therefore cause a gradual increase in floc size and volumetric fraction as the flocculation test proceeds. In this case, the intact fraction of flocculi at equilibrium is smaller than 20%. Second, the particle scavenging mechanism of the microbial backbones might govern the flocculation kinetic tests in the stationary phase (i.e., 30 d of microalgal incubation time). An excessive quantity of biopolymers produced by the microalgal cells in the stationary phase might produce many microbial and polymeric backbones and cause fast flocculation kinetics initially. However, accumulation of an excessive quantity of biopolymers and HS in the stationary phase might enhance stabilization of flocculi, leading to the retention of a large amount (~37%) of intact flocculi at equilibrium. Biopolymers can be attributed to the formation of large, aggregation-prone backbone structures within algal cells. However, simultaneously, the accumulation of biopolymers and HS might enhance stabilization because of steric stabilization in that adsorbed polymeric layers on the particle surfaces provide additional repulsive force between particles (Healy and Mer, 1962; Lee et al., 2012b).

Biologically mediated flocculation of microalgae and clay minerals depends on physicochemical characteristics of water, such as pH and salinity (Mietta et al., 2009; Sengco and Anderson, 2004). Abundant protons in low (acidic) pH conditions can accumulate on the surfaces of clay mineral platelets and neutralize the surface charge and electrostatic repulsion. The pH also controls protolytic reactions at the hydroxyl functional sites on the edges of clay minerals, thus changing the surface

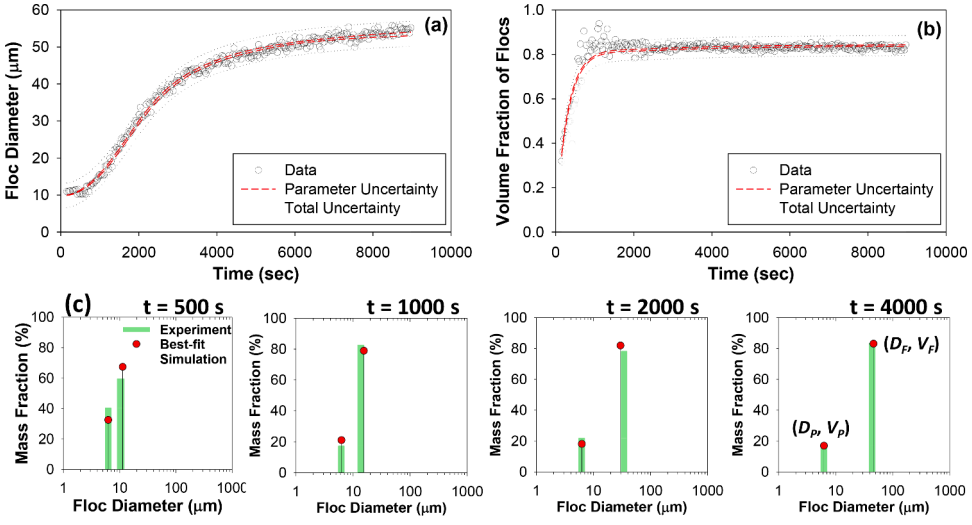

Fig. 8. Time series of (a) the floc diameter and (b) the floc volumetric fraction with 95% simulation uncertainty intervals due to parameter and total uncertainty, for the flocculation kinetic test at 13 d of microalgal incubation time. (c) the separate peaks of flocculi and flocs, measured and simulated at 500, 1000, 2000, and 4000 s in the flocculation kinetic test. In (c), D_P and V_P indicate the mean sizes and volumetric fraction of flocculi, and D_F and V_F indicate those of flocs.

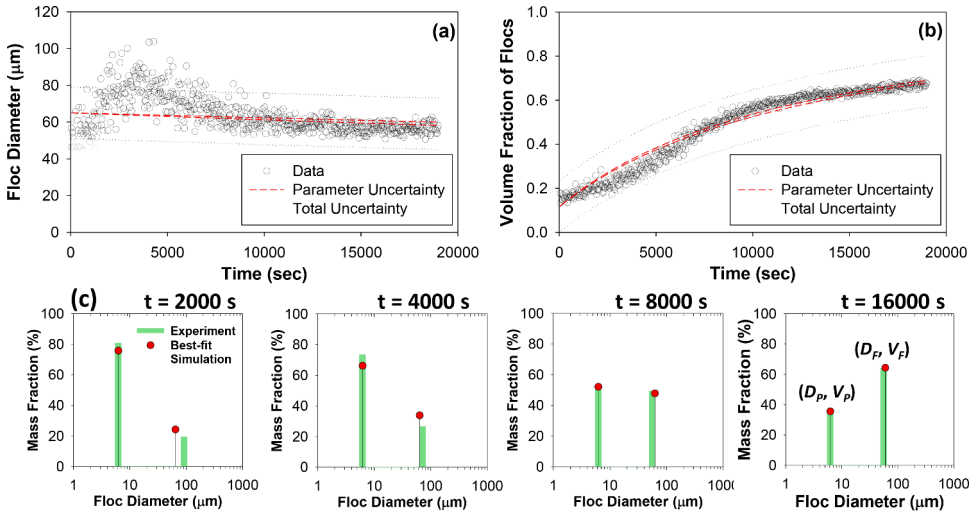

Fig. 9. Time series of (a) the floc diameter and (b) the floc volumetric fraction with 95% simulation uncertainty intervals due to parameter and total uncertainty, for the flocculation kinetic test at 30 d of microalgal incubation time. (c) the separate peaks of flocculi and flocs, measured and simulated after 2000, 4000, 8000, and 16000 s in the flocculation kinetic test. In (c), D_P and V_P indicate the mean sizes and volumetric fraction of flocculi, and D_F and V_F indicate those of flocs.

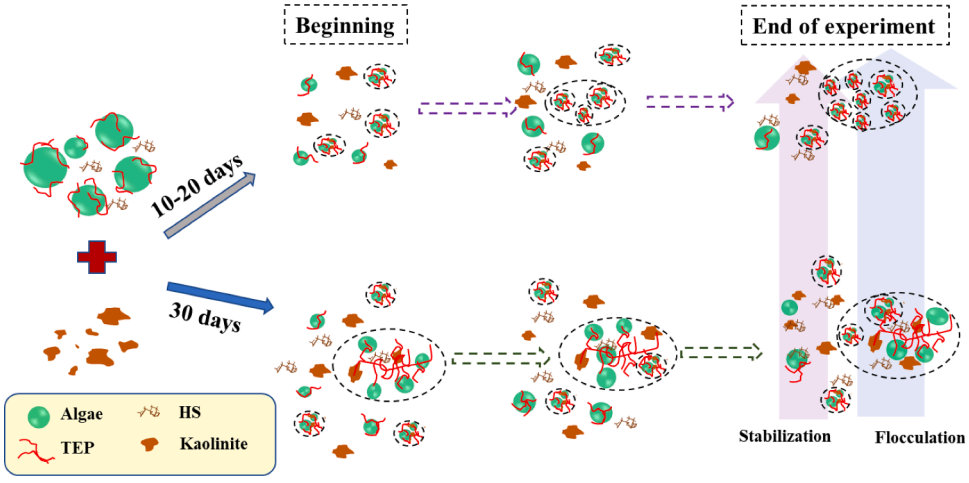

Fig. 10. Schematic diagram describing the model conception of flocculation occurring in the microalgae- and kaolinite-containing suspension during the exponential growth (i.e., 10–20 d) and stationary phases (i.e., 30 d) of microalgal growth.

charge and electrostatic property of particles/flocs and determining the flocculation potential of microalgae and clays (Tombácz and Szekeres, 2006). Salinity also affects the flocculation potential, as high salinity decreases the surface charge and repulsive force of particles/flocs, thereby enhancing flocculation (Mietta et al., 2009). However, the effects of pH and salinity on flocculation are highly complex under various aquatic environments (Eisma et al., 1991; van Leussen, 1999). This study was initiated at pH and salinity of 7 and 0.01 M NaCl, respectively, as a proxy for terrestrial water. Therefore, follow-up studies should apply a wide range of pH and salinity conditions, replicating the terrestrial, brackish, and saline water environments, to investigate the effect of pH and salinity on the biologically mediated flocculation of microalgae and clays.

4. Conclusions

The results of this study elucidate the flocculation kinetics of microalgae and clay-containing suspensions. Our results indicate that the microalgae growth phase, OM composition, and flocculation potential are closely related. The findings of this study are summarized as follows:

1 The FSDs of the microalgae- and clay-containing suspensions showed typical two-class flocculation kinetics, in which the size and volumetric fraction of flocs (D_F and V_F) increased with time, whereas the volumetric fraction of flocculi (V_P) decreased while maintaining a narrow size range.

2 Flocculation kinetics were found to depend on the quantity of different OM fractions (e.g., biopolymers, HS) produced by microalgae. An adequate quantity of biopolymer in the algal growth phase promoted floc-to-floc attachment and enhanced the flocculation kinetics of the microalgae- and clay-containing suspensions. In contrast, an excessive quantity of biopolymers and HS in the stationary phase promoted sweeping flocculation with large polymeric backbone structures but simultaneously enhanced steric stabilization by increasing the repulsive force of the biopolymer and HS attachment on the particle surfaces.

3 The two-class flocculation kinetic model with Bayesian calibration could further demonstrate the distinct flocculation and stabilization mechanisms: (1) floc-to-floc collision and attachment in the microalgae growth phase, and (2) backbone-induced sweeping flocculation and steric stabilization in the stationary phase.

Flocculation is critical in water resource management to determine the fate and transport of SPM. Flocculation is involved in the sinking of various substances (e.g., SPM, heavy metals, nutrients, and OM) in the water column down to the river or lake beds, while it is influenced by various biogeochemical characteristics (e.g., DOM quality and quantity). The findings of this study could improve the understanding of complex aquatic processes, especially flocculation, sedimentation, and transportation of SPM in water resources that affect the quantity and quality of water and benthic environments.

Funding

This work was supported by the National Research Foundation of Korea (Project No. NRF-2020R1I1A3A04036895) and K-water Corporation (Project No. 21-BW-005).

Declaration of Competing Interest

The authors declare that they have no known competing financial interests or personal relationships that could have appeared to influence the work reported in this paper.

The authors declare the following financial interests/personal relationships which may be considered as potential competing interests:

We wish to confirm that there are no known conflicts of interest associated with this manuscript.

Data availability

Data will be made available on request.

Acknowledgments

We appreciate the financial support of the National Research Foundation of Korea (Project No. NRF-2020R1I1A3A04036895) and K-water Corporation (Project No. 21-BW-005). Scientific input from Michael Fettweis and Xavier Desmit is integrated into the research programs BGPART supported by the Belgian Science Policy (BELSPO) within the BRAIN-be program, and MOMO supported by the Maritime Access Division of the Flemish Ministry of Mobility and Public Works.

Supplementary materials

Supplementary material associated with this article can be found, in the online version, at doi:10.1016/j.watres.2022.119300.

References

Alldredge, A.L., Silver, M.W., 1988. Characteristics, dynamics and significance of marine snow. Prog. Oceanogr. 20 (1), 41–82.
Avnimelech, Y., Menzel, R.G., 1984. Coflocculation of algae and clay to clarify turbid impoundments. J. Soil Water Conserv. 39 (3), 200–203.
Avnimelech, Y., Troeger, B.W., Reed, L.W., 1982. Mutual flocculation of algae and clay: evidence and implications. Science 216 (4541), 63–65.
Babiak, W., Krzemińska, I., 2021. Extracellular polymeric substances (EPS) as microalgal bioproducts: a review of factors affecting EPS synthesis and application in flocculation processes. Energies 14 (13), 4007.
Beckers, F., Heredia, A., Noack, M., Nowak, W., Wieprecht, S., Oladyshkin, S., 2020. Bayesian calibration and validation of a large-scale and time-demanding sediment transport model. Water Resour. Res. 56 (7), e2019WR026966.
Burd, A.B., Jackson, G.A., 2002. Modeling steady-state particle size spectra. Environ. Sci. Technol. 36 (3), 323–327.
Chin, W.-C., Orellana, M.V., Verdugo, P., 1998. Spontaneous assembly of marine dissolved organic matter into polymer gels. Nature 391 (6667), 568–572.
Chioccioli, M., Hankamer, B., Ross, I.L., 2014. Flow cytometry pulse width data enables rapid and sensitive estimation of biomass dry weight in the microalgae Chlamydomonas reinhardtii and Chlorella vulgaris. PLoS One 9 (5), e97269.
Dallmann, J., Phillips, C., Teitelbaum, Y., Sund, N., Schumer, R., Arnon, S., Packman, A., 2020. Impacts of suspended clay particle deposition on sand-bed morphodynamics. Water Resour. Res. 56 (8), e2019WR027010.
de Lucas Pardo, M.A., Sarpe, D., Winterwerp, J.C., 2015. Effect of algae on flocculation of suspended bed sediments in a large shallow lake. Consequences for ecology and sediment transport processes. Ocean Dyn. 65 (6), 889–903.
Deng, Z., 2022. The Role of Algae in Fine Cohesive Sediment Flocculation (Ph.D. Dissertation). TU Delft, The Netherlands.
Deng, Z., He, Q., Safar, Z., Chassagne, C., 2019. The role of algae in fine sediment flocculation: in-situ and laboratory measurements. Mar. Geol. 413, 71–84.
Diaz, R.J., Rosenberg, R., 2008. Spreading dead zones and consequences for marine ecosystems. Science 321 (5891), 926–929.
Droppo, I.G., 2001. Rethinking what constitutes suspended sediment. Hydrol. Processes 15 (9), 1551–1564.
Drummond, J., Aubeneau, A., Packman, A., 2014. Stochastic modeling of fine particulate organic carbon dynamics in rivers. Water Resour. Res. 50 (5), 4341–4356.
Ducklow, H., 1993. Bacterial production in estuaries. Aquatic Microbiology—an Ecological Approach. Blackwell Scientific Publications, Boston, MA, USA, pp. 261–287.
Eisma, D., Bernard, P., Cadée, G., Ittekkot, V., Kalf, J., Laane, R., Martin, J., Mook, W., Van Put, A., Schuhmacher, T., 1991. Suspended-matter particle size in some west-European estuaries—part II: a review on floc formation and break-up. Neth. J. Sea Res. 28 (3), 215–220.
Engel, A., Thoms, S., Riebesell, U., Rochelle-Newall, E., Zondervan, I., 2004. Polysaccharide aggregation as a potential sink of marine dissolved organic carbon. Nature 428 (6986), 929–932.
Fagel, N., 2007. Chapter four clay minerals, deep circulation and climate. Dev. Mar. Geol. 1, 139–184.
Fettweis, M., Baeye, M., 2015. Seasonal variation in concentration, size, and settling velocity of muddy marine flocs in the benthic boundary layer. J. Geophys. Res. 120 (8), 5648–5667.
Fettweis, M., Schartau, M., Desmit, X., Lee, B.J., Terseleer, N., Van der Zande, D., Parmentier, K., Riethmüller, R., 2022. Organic matter composition of biomineral flocs and its influence on suspended particulate matter dynamics along a nearshore to offshore transect. J. Geophys. Res. 127 (1), e2021JG006332.
Fogg, G., 1977. Excretion of organic matter by phytoplankton. Limnology and Oceanography 22 (3), 576–577.
Gep, B., Tiao, G., 1973. Bayesian Inference in Statistical Analysis. Reading Addison-Wesley, New York, USA.
Giorgi, F., Coglitore, D., Curran, J.M., Gilliland, D., Macko, P., Whelan, M., Worth, A., Patterson, E.A., 2019. The influence of inter-particle forces on diffusion at the nanoscale. Sci. Rep. 9 (1), 1–6.
Healy, T.W., Mer, V.K.L., 1962. The adsorption-flocculation reactions of a polymer with an aqueous colloidal dispersion. J. Phys. Chem. 66 (10), 1835–1838.
Huber, S.A., Balz, A., Abert, M., Pronk, W., 2011. Characterisation of aquatic humic and non-humic matter with size-exclusion chromatography–organic carbon detection–organic nitrogen detection (LC-OCD-OND). Water Res. 45 (2), 879–885.
Hussein, T., 2005. Indoor and Outdoor Aerosol Particle Size Characterization in Helsinki. University of Helsinki, Finland.
Jacquet, S., Briand, J.-F., Leboulanger, C., Avois-Jacquet, C., Oberhaus, L., Tassin, B., Vinçon-Leite, B., Paolini, G., Druart, J.-C., Anneville, O., 2005. The proliferation of the toxic cyanobacterium Planktothrix rubescens following restoration of the largest natural French lake (Lac du Bourget). Harmful Algae 4 (4), 651–672.
Kim, Z.-H., Thanh, N.N., Yang, J.-H., Park, H., Yoon, M.-Y., Park, J.-K., Lee, C.-G., 2016. Improving microalgae removal efficiency using chemically-processed clays. Biotechnol. Bioprocess Eng. 21 (6), 787–793.
Kiørboe, T., Andersen, K., Dam, H., 1990. Coagulation efficiency and aggregate formation in marine phytoplankton. Mar. Biol. 107 (2), 235–245.
Kiørboe, T., Lundsgaard, C., Olesen, M., Hansen, J.L., 1994. Aggregation and sedimentation processes during a spring phytoplankton bloom: a field experiment to test coagulation theory. J. Mar. Res. 52 (2), 297–323.
Lee, B.J., Fettweis, M., Toorman, E., Molz, F.J., 2012a. Multimodality of a particle size distribution of cohesive suspended particulate matters in a coastal zone. J. Geophys. Res.: Ocea. 117 (C3), C03014.
Lee, B.J., Hur, J., Toorman, E.A., 2017. Seasonal variation in flocculation potential of river water: roles of the organic matter pool. Water 9 (5), 335.
Lee, B.J., Schlautman, M.A., Toorman, E., Fettweis, M., 2012b. Competition between kaolinite flocculation and stabilization in divalent cation solutions dosed with anionic polyacrylamides. Water Res. 46 (17), 5696–5706.
Lee, B.J., Toorman, E., Molz, F.J., Wang, J., 2011. A two-class population balance equation yielding bimodal flocculation of marine or estuarine sediments. Water Res. 45 (5), 2131–2145.
Liu, Y., Cao, X., Yu, Z., Song, X., Qiu, L., 2016. Flocculation of harmful algal cells using modified clay: effects of the properties of the clay suspension. J. Appl. Phycol. 28 (3), 1623–1633.
Maggi, F., 2005. Flocculation dynamics of cohesive sediment (Ph.D. Dissertation). TU Delft, The Nertherlands.
Maggi, F., 2009. Biological flocculation of suspended particles in nutrient-rich aqueous ecosystems. J. Hydrol. 376 (1-2), 116–125.
Manning, A., Baugh, J., Soulsby, R., Spearman, J., Whitehouse, R., 2011. Cohesive Sediment Flocculation and the Application to Settling Flux Modelling. Sediment Transport. IntechOpen, London, UK, pp. 91–116.
Mietta, F., Chassagne, C., Manning, A.J., Winterwerp, J.C., 2009. Influence of shear rate, organic matter content, pH and salinity on mud flocculation. Ocean Dyn. 59 (5), 751–763.
Nagata, T., 2000. Production mechanisms of dissolved organic matter. Microbial Ecology of the Oceans. John Wiley & Sons, New York, USA, pp. 121–152.

Nakayama, S., Sakamoto, Y., Yamaguchi, T., Akai, M., Tanaka, T., Sato, T., Iida, Y., 2004. Dissolution of montmorillonite in compacted bentonite by highly alkaline aqueous solutions and diffusivity of hydroxide ions. Appl. Clay Sci. 27 (1-2), 53–65.
Neumann, A., Hass, H.C., Möbius, J., Naderipour, C., 2019. Ballasted flocs capture pelagic primary production and alter the local sediment characteristics in the coastal German Bight (North Sea). Geosciences 9 (8), 344.
Nguyen, M.-L., Westerhoff, P., Baker, L., Hu, Q., Esparza-Soto, M., Sommerfeld, M., 2005. Characteristics and reactivity of algae-produced dissolved organic carbon. J. Environ. Eng. 131 (11), 1574–1582.
Nosaka, Y., Yamashita, Y., Suzuki, K., 2017. Dynamics and origin of transparent exopolymer particles in the Oyashio region of the western subarctic Pacific during the spring diatom bloom. Front. Mar. Sci. 4, 79.
Partheniades, E., 2009. Cohesive Sediments in Open Channels: Erosion, Transport and Deposition. Butterworth-Heinemann, Oxford, UK.
Passow, U., 2002. Transparent exopolymer particles (TEP) in aquatic environments. Prog. Oceanogr. 55 (3-4), 287–333.
Passow, U., Alldredge, A., 1995. A dye-binding assay for the spectrophotometric measurement of transparent exopolymer particles (TEP). Limnol. Oceanogr. 40 (7), 1326–1335.
Preisner, M., Neverova-Dziopak, E., Kowalewski, Z., 2021. Mitigation of eutrophication caused by wastewater discharge: a simulation-based approach. Ambio 50 (2), 413–424.
Sengco, M.R., Anderson, D.M., 2004. Controlling harmful algal blooms through clay flocculation 1. J. Eukaryot. Microbiol. 51 (2), 169–172.
Sharp, J.H., 1977. Excretion of organic matter by marine phytoplankton: do healthy cells do it? 1. Limnol. Oceanogr. 22 (3), 381–399.
Shemesh, A., Zvulunov, Y., Radian, A., 2021. Impact of cocultivation on the aggregation and sedimentation trends of cyanobacteria with native and modified clay minerals. Sep. Purif. Technol. 278, 119179.
Shi, W., Tan, W., Wang, L., Pan, G., 2016. Removal of Microcystis aeruginosa using cationic starch modified soils. Water Res. 97, 19–25.
Sionneau, T., Bout-Roumazeilles, V., Biscaye, P., van Vliet-Lanoë, B., Bory, A., 2008. Clay mineral distributions in and around the Mississippi River watershed and Northern Gulf of Mexico: sources and transport patterns. Quat. Sci. Rev. 27 (17-18), 1740–1751.
Spencer, K.L., Wheatland, J.A., Bushby, A.J., Carr, S.J., Droppo, I.G., Manning, A.J., 2021. A structure–function based approach to floc hierarchy and evidence for the non-fractal nature of natural sediment flocs. Sci. Rep. 11 (1), 1–10.
Stevenson, K., McVey, A.F., Clark, I.B., Swain, P.S., Pilizota, T., 2016. General calibration of microbial growth in microplate readers. Sci. Rep. 6 (1), 1–7.
Tang, F., 2016. Microbiological modulation of suspended particulate matter dynamics: A study of biological flocculation in nutrient-enriched waters (Ph.D. Dissertation). The University of Sydney, Australia. PhD thesis.
Tombácz, E., Szekeres, M., 2006. Surface charge heterogeneity of kaolinite in aqueous suspension in comparison with montmorillonite. Appl. Clay Sci. 34 (1-4), 105–124.
US Environmental Protection Agency, 2001. Total, Fixed, and Volatile Solids in Water, Solids, and Biosolids. Clean Water Act Analytical Methods. US EPA, Washington, USA.
Van Leussen, W., 1994. Esturine Macroflocs: their Role in Fine Grained Sediment Transport, 488. University of Utrecht, Utrecht.
van Leussen, W., 1999. The variability of settling velocities of suspended fine-grained sediment in the Ems estuary. J. Sea Res. 41 (1-2), 109–118.
Verspagen, J.M., Visser, P.M., Huisman, J., 2006. Aggregation with clay causes sedimentation of the buoyant cyanobacteria Microcystis spp. Aquat. Microb. Ecol. 44 (2), 165–174.
Villacorte, L.O., 2014. Algal blooms and membrane based desalination technology (Ph.D. Dissertation). TU Delft, The Nertherland.
Villacorte, L.O., Ekowati, Y., Calix-Ponce, H.N., Schippers, J.C., Amy, G.L., Kennedy, M. D., 2015. Improved method for measuring transparent exopolymer particles (TEP) and their precursors in fresh and saline water. Water Res. 70, 300–312.
Villacorte, L.O., Kennedy, M.D., Amy, G.L., Schippers, J.C., 2009. The fate of Transparent Exopolymer Particles (TEP) in integrated membrane systems: removal through pre-treatment processes and deposition on reverse osmosis membranes. Water Res. 43 (20), 5039–5052.
Vrugt, J.A., Ter Braak, C., Diks, C., Robinson, B.A., Hyman, J.M., Higdon, D., 2009. Accelerating Markov chain Monte Carlo simulation by differential evolution with self-adaptive randomized subspace sampling. Int. J. Nonlinear Sci. Numer. Simul. 10 (3), 273–290.
Walch, H., von der Kammer, F., Hofmann, T., 2022. Freshwater Suspended Particulate Matter–Key Components and Processes in Floc Formation and Dynamics. Water Res. 118655, 135.
Wei, C., Liao, Q., Huang, Y., Zhu, X., Xia, A., Zhu, X., 2020. Simultaneous enhancing the sedimentation and adsorption performance of Chlorella vulgaris with montmorillonite modified cationic starch. Biochem. Eng. J. 164, 107785.
Weisstein, E.W., 2001. Triangular Distribution. Wolfram MathWorld, Wolfram Web Resource. https://mathworld.wolfram.com/.
Whitby, K.T., 1967. The physical characteristics of sulfur aerosols. Atmosp. Environ. 12 (1-3), 135–159.
Winterwerp, J.C., 1998. A simple model for turbulence induced flocculation of cohesive sediment. J. Hydraul. Res. 36 (3), 309–326.
Xiao, R., Zheng, Y., 2016. Overview of microalgal extracellular polymeric substances (EPS) and their applications. Biotechnol. Adv. 34 (7), 1225–1244.
Yin, Z., Li, S., Hu, D., Li, Z., Chu, R., Liu, C., Li, X., Hu, J., Zhu, L., 2022. Performance evaluation of different chitosan-clay composite materials for efficient harvesting of Chlorella vulgaris and impacts on downstream bioproduct processing and water reusability. Chem. Eng. J. 430, 132892.